Bioorganic Chemistry 93 (2019) 103310

Contents lists available at ScienceDirect

Bioorganic Chemistry

journal homepage: www.elsevier.com/locate/bioorg

Design, synthesis, biological evaluation, and molecular modeling studies of quinoline-ferulic acid hybrids as cholinesterase inhibitors

Jun Mo[b,1], Hongyu Yang[b,1], Tingkai Chen[c], Qihang Li[b], Hongzhi Lin[b], Feng Feng[c,f], Wenyuan Liu[d], Wei Qu[c], Qinglong Guo[e], Heng Chi[f], Yao Chen[a,*], Haopeng Sun[b,f,*]

[a] School of Pharmacy, Nanjing University of Chinese Medicine, Nanjing 210023, People's Republic of China
[b] Department of Medicinal Chemistry, School of Pharmacy, China Pharmaceutical University, Nanjing 211198, People's Republic of China
[c] Department of Natural Medicinal Chemistry, China Pharmaceutical University, Nanjing 211198, People's Republic of China
[d] Department of Pharmaceutical Analysis, Key Laboratory of Drug Quality Control and Pharmacovigilance, Ministry of Education, China Pharmaceutical University, Nanjing 210009, People's Republic of China
[e] State Key Laboratory of Natural Medicines, Jiangsu Key Laboratory of Carcinogenesis and Intervention, School of Basic Medicine and Clinical Pharmacy, China Pharmaceutical University, Nanjing 210009, People's Republic of China
[f] Jiangsu Food and Pharmaceuticals Science College, Institute of Food and Pharmaceuticals Research, 223005, People's Republic of China

ARTICLE INFO

Keywords:
Alzheimer's disease
Cholinesterase inhibitor
Quinoline-ferulic acid hybrid
Molecular docking

ABSTRACT

A series of quinoline-ferulic acid hybrids has been designed, synthesized, and evaluated as cholinesterase inhibitors. Most of the compounds showed good inhibitory activities toward both acetylcholinesterase (AChE) and butyrylcholinesterase (BChE). Among them, **10f** was found to be the most potent inhibitor against AChE (IC_{50} = 0.62 ± 0.17 μM), and **14** was the most potent inhibitor against BChE (IC_{50} = 0.10 ± 0.01 μM). Representative compounds, such as **10f** and **12g**, act in a competitive manner when they inhibit AChE or BChE. Molecular docking and dynamic simulation revealed that the synthesized compounds bind to the target by simultaneously interacting with the catalytic active site (CAS) and the peripheral anionic site (PAS) of both AChE and BChE. The U-shaped confirmation was preferred when **12g** bound to BChE, which was different from the linear conformation of **10f** bound to AChE. Cell-based assays have confirmed the moderate neuroprotective effects of compounds **10f** and **12g** against H_2O_2-induced oxidative damage towards PC12 cells. Moreover, the hepatotoxicity of **12g** was lower than that of tacrine, indicating its potential safety as an anti-Alzheimer's agent. In summary, we report a new chemotype of multifunctional hybrid, which may be further modified to develop new anti-Alzheimer's agents.

1. Introduction

Alzheimer's disease (AD) is an age-related neurodegenerative disease characterized by a progressive loss of cognitive abilities, such as memory, language skills, and attention span, leading to disorientation and depression [1]. AD is estimated to incur a global annual expenditure of two trillion dollars by 2030 [2]. Currently, only four drugs have been approved by the U.S. Food and Drug Administration (FDA) for the treatment of AD, namely donepezil, rivastigmine, galantamine, and memantine [3]. However, the therapeutic effects of these drugs are limited, so there is an urgent demand to develop new therapeutic agents for AD [4,5].

The cholinergic system, which plays an important role in the regulation of learning, cognition, and memory processes [6], has been extensively studied for the design of anti-AD drugs [7,8]. Indeed, cholinergic dysfunction has been identified as one of the major causes of AD. Acetylcholine (ACh) can be hydrolyzed by two types of cholinesterases (ChEs): acetylcholinesterase (AChE) and butyrylcholinesterase (BChE) [9]. During the early stage of AD, AChE plays a dominant role in ACh hydrolysis, while BChE plays only a supportive role [10,11]. Therefore, inhibiting the activity of AChE is an effective way to ameliorate cognitive dysfunction in AD. However, studies have shown that compounds that are able to inhibit BChE may offer an alternative role for the treatment of AD, especially in its advanced stage [12]. During the development of AD, the BChE/AChE ratio gradually increases, partially as a consequence of a progressive loss of the cholinergic synapses in which AChE resides [13].

* Corresponding authors at: School of Pharmacy, Nanjing University of Chinese Medicine, Nanjing 210023, People's Republic of China (Y. Chen). Department of Medicinal Chemistry, School of Pharmacy, China Pharmaceutical University, Nanjing 211198, People's Republic of China (H. Sun).
E-mail addresses: clarissa0710@163.com (Y. Chen), sunhaopeng@163.com (H. Sun).
[1] These two authors contributed equally to this paper.

https://doi.org/10.1016/j.bioorg.2019.103310
Received 6 December 2018; Received in revised form 4 September 2019; Accepted 22 September 2019
Available online 23 September 2019
0045-2068/

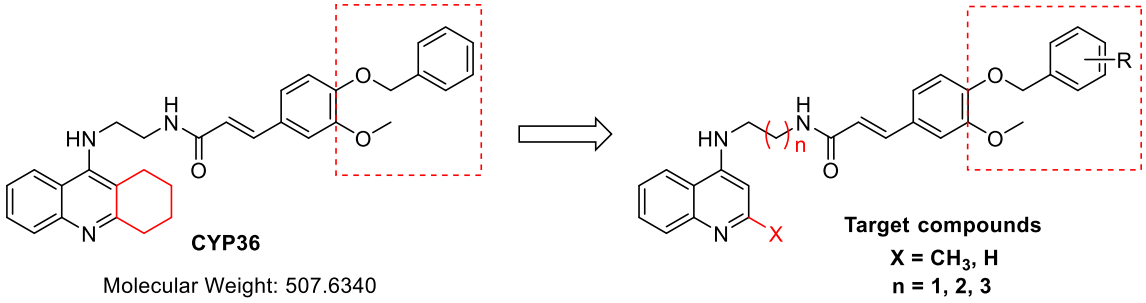

Fig. 1. Design of a series of quinoline-ferulic acid hybrids as cholinesterase inhibitors.

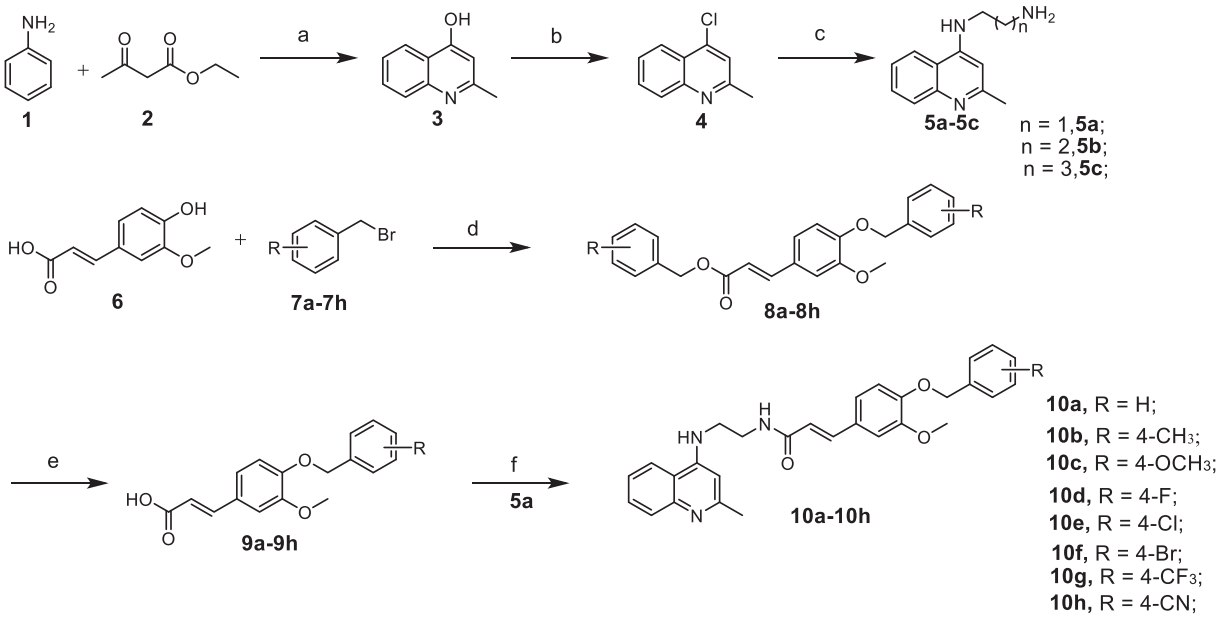

Scheme 1. Reagents and conditions: (a) PPA, 130 °C, 3 h; (b) $POCl_3$, reflux, 2 h; (c) phenol, sodium iodide, 120 °C; (d) K_2CO_3, DMF, 85 °C, 5 h; (e) NaOH, MeOH, H_2O, 85 °C, 3 h; (f) PyBOP, DIPEA, DMF, 4 h, rt.

Multi-target-directed ligands (MTDLs) can display multiple bioactivities by simultaneously regulating different nodes or pathways. Considering the multifactorial nature of AD, MTDLs are supposed to exhibit promising therapeutic effects, therefore, it is considered to be an important strategy for the development of anti-AD drugs [14]. Our group has focused on the design and synthesis of new MTDLs in recent years. Previously, we disclosed a series of tacrine-cinnamic acid hybrids/tacrine-ferulic acid hybrids (**CYP36**, Fig. 1) as MTDLs against AD [15,16]. In these publications, we focused our attention on modifications of the cinnamic acid/ferulic acid moieties, as well as the choice of linker in these hybrids. Although these hybrids showed good multifunctional activity as desired, the chemotype of the hybrids remained limited, and structure–activity relationships (SAR), especially of the tacrine moiety, were not comprehensively studied. We surmised that the complicated structure of these hybrids may lead to undesirable physicochemical properties, which may hinder their further development. Hence, further structural modification and SAR studies were deemed necessary. Herein, we disclose the results of structural modification on a 1,2,3,4-tetrahydroacridine moiety. To simplify the structures of the hybrids, the cyclohexyl part of 1,2,3,4-tetrahydroacridine moiety was removed, leading to a series of compounds with quinoline core. The resultant hybrids retained multifunctional activity according to biological assays, indicating that removal of the cyclohexyl part of the 1,2,3,4-tetrahydroacridine moiety is tolerable for medicinal chemistry modification. The obtained anti-AD hybrids with a new chemotype, such as a quinoline-cinnamic acid scaffold (Fig. 1), may represent an alternative starting point for subsequent optimization as new bioactive compounds for AD treatment. Additionally, the slightly reduced molecular weight of the compounds, compared to those reported previously, is also preferable for drug development.

In the present study, the inhibitory activities of the quinoline-cinnamic acid hybrids on AChE and BChE have been investigated. To further determine the binding mode of the target molecules on AChE and BChE, kinetic, molecular docking, and molecular dynamics (MD) experiments have been performed on selected compounds. The multifunctional properties of the compounds, including their effects on self-mediated Aβ aggregation, antioxidant activities, and neuroprotection, have been determined *in vitro* or in cell-based assays. The hepatotoxicity of the hybrids has been evaluated to show their potential safety as anti-AD agents.

This study identifies a new scaffold for the further design of MTDLs against AD. The SAR results, especially the tolerance to modification of the quinoline core, suggest that further optimization of the substituent thereon, or even replacement of the ring with another heterocycle, merits further study.

2. Results and discussion

2.1. Chemistry

The synthetic route to quinoline-ferulic acid hybrids **10a–10h** is shown in Scheme 1. 2-Methyl-4-hydroxylquinoline (**3**) was prepared by the condensation of aniline with ethyl acetoacetate catalyzed by polyphosphoric acid (PPA) at 130 °C. Compound **3** was then treated with

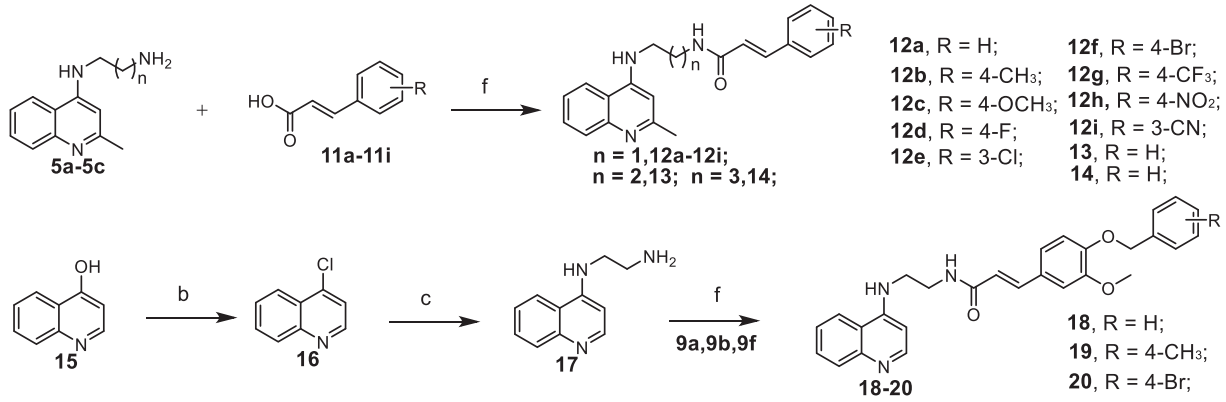

Scheme 2. Reagents and conditions: (b) $POCl_3$, reflux, 2 h; (c) phenol, sodium iodide, 120 °C; (f) PyBOP, DIPEA, DMF, 4 h, rt.

Table 1
Structures and eeAChE and eqBChE inhibitory activities of the target compounds.

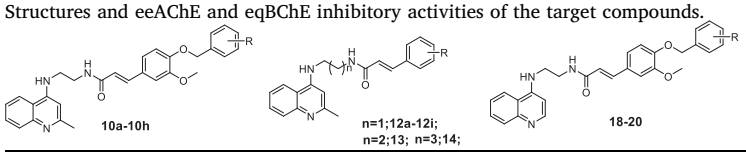

Compound	n	R	IC_{50} (μM) ± SEM[a]	
			AChE[b]	BChE[c]
10a	–	H	1.43 ± 0.32	3.38 ± 0.77
10b	–	4-CH_3	1.69 ± 0.62	3.37 ± 0.13
10c	–	4-OCH_3	3.46 ± 0.67	1.09 ± 0.67
10d	–	4-F	6.59 ± 0.95	0.99 ± 0.54
10e	–	4-Cl	1.61 ± 0.16	9.13 ± 1.16
10f	–	4-Br	0.62 ± 0.17	1.18 ± 0.14
10g	–	4-CF_3	1.59 ± 0.58	1.19 ± 0.36
10h	–	4-CN	1.07 ± 0.47	0.87 ± 0.17
12a	1	H	5.51 ± 2.90	1.33 ± 1.41
12b	1	4-CH_3	2.62 ± 0.88	2.11 ± 0.46
12c	1	4-OCH_3	2.44 ± 1.27	2.17 ± 0.37
12d	1	4-F	4.07 ± 1.77	7.07 ± 1.32
12e	1	4-Cl	3.38 ± 0.95	1.58 ± 0.52
12f	1	4-Br	3.54 ± 1.12	1.51 ± 0.28
12g	1	4-CF_3	3.28 ± 1.32	0.93 ± 0.40
12h	1	4-NO_2	1.45 ± 0.62	4.04 ± 1.85
12i	1	3-CN	10.04 ± 5.99	3.05 ± 0.85
13	2	H	1.35 ± 0.41	0.58 ± 0.15
14	3	H	2.47 ± 0.37	0.10 ± 0.01
18	–	H	3.69 ± 0.66	2.43 ± 0.78
19	–	4-CH_3	1.06 ± 0.23	1.04 ± 0.36
20	–	4-Br	1.44 ± 0.41	0.44 ± 0.14
Tacrine			0.02 ± 0.01	0.008 ± 0.004

[a] Concentration required for 50% inhibition of ChEs; data are shown as the mean ± SEM of triplicate independent experiments.
[b] AChE (EC 3.1.1.7) from electric eel.
[c] BChE (EC 3.1.1.8) from horse serum.

phosphoryl chloride at 120 °C for 2 h to give 4-chloro-2-methylquinoline (**4**). Next, compound **4** was treated with ethylenediamine or 1,3-propanediamine or 1,4-diaminobutane at 120 °C for 10 h to give intermediates **5a–5c**. The intermediates **8a–8h** were prepared by condensation reactions of ferulic acid (**6**) with various substituted benzyl bromides (**7a–7h**) at 85 °C for 5 h. The benzyl groups of **8a–8h** were removed by treatment with 2 N aq. NaOH to obtain intermediates **9a–9h**. Finally, the intermediates **9a–9h** were reacted with compound **5a** at room temperature to obtain the target molecules **10a–10h**.

The synthetic route to quinoline-cinnamic acid hybrids **12a–12i**, **13**, and **14** is shown in Scheme 2. The intermediates **5a–5c** were reacted with various cinnamic acid derivatives (**11a–11i**) at room temperature to afford the target molecules **12a–12i**, **13**, and **14**.

The synthetic route to quinoline-ferulic acid hybrids **18–20** is also shown in Scheme 2. 4-Hydroxylquinoline (**15**) was treated with phosphoryl chloride at 120 °C for 2 h to give 4-chloroquinoline (**16**). Next, compound **16** was treated with ethylenediamine at 120 °C for 10 h to give N^1-(quinolin-4-yl)ethane-1,2-diamine (**17**). The intermediate **17** was reacted with intermediates **9a**, **9b**, or **9f** at room temperature to afford the target molecules **18–20**.

2.2. Pharmacology

2.2.1. AChE and BChE inhibitory activities of the target molecules

The inhibitory effects of all of the synthesized compounds on AChE from eeAChE and BChE from eqBChE were assayed according to the

modified method of Ellman et al. [17]. Most of the compounds proved to be potent inhibitors of AChE and BChE. The results are expressed in terms of IC_{50} values (Table 1).

Firstly, we synthesized quinoline-ferulic acid hybrids (**10a–10h**). Compared to **10a**, we introduced 4-methyl (**10b**) and 4-methoxyl (**10c**) groups on the benzyloxyl moiety. **10b** showed comparable activity to **10a**, whereas **10c** showed slightly reduced activity towards AChE, but improved inhibitory activity towards BChE. We then designed compounds with different halogen atom substitutions. **10d** showed selectivity towards BChE, whereas **10e** exhibited selectivity towards AChE. Compared to **10a**, **10f** showed improved activity towards both AChE and BChE. The activity towards AChE decreased in the order 4-Br (**10f**) > 4-Cl (**10e**) > 4-F (**10d**). Subsequently, we explored the inductive effects of substituents on ChE inhibitory activities. Compared to the electron-donating groups 4-CH_3 and 4-OCH_3, electron-withdrawing groups such as 4-CF_3 (**10g**) and 4-CN (**10h**) enhanced AChE and BChE inhibitory activities.

Next, we synthesized quinoline-cinnamic acid hybrids (**12a–12i**, **13**, and **14**). Compared to quinoline-ferulic acid hybrids (**10a–10h**), they showed similar activities and target selectivities. We introduced 4-methyl and 4-methoxyl groups on the cinnamic acid moiety. **12b** and **12c** showed reduced BChE inhibitory activities, but were favorable for AChE inhibition. The impact of halogen atoms on the ChE inhibition was also evaluated for this series of compounds. For the different halo-substituted derivatives, the activities towards BChE decreased in the order 4-Br (**12f**) > 4-Cl (**12e**) > 4-F (**12d**), as for the ferulic acid counterparts mentioned above. It is noteworthy that compound **12d**, with 4-F as the substitution, showed reduced activity towards AChE inhibition, similarly to compound **10d**. The results indicate that F is not favorable for enhancing the AChE inhibitory activity. Next, $-CF_3$ (**12g**), $-NO_2$ (**12h**), and −CN (**12i**), as three electron-withdrawing groups, were introduced. These three compounds showed activities comparable to that of **12a**. The results suggested that the electron-inductive effect does not have an impact on the ChE inhibitory activities of the target compounds, implying a tolerance for such structure modification. Next, we explored the effect of linker length on ChE inhibitory activities. Compound **13** incorporating a three-carbon chain showed increased AChE and BChE inhibitory activities compared to compound **12a**. When a four-carbon chain was introduced, compound **14** also exhibited enhanced AChE and BChE inhibitory activities.

Subsequently, we synthesized **18**, **19**, and **20**, which lack the methyl group on the quinoline ring of **10a**. **18** showed comparable activity to **10a**, indicating that the methyl group on the quinoline ring is not important for the activity. To confirm this result, we further synthesized 4-methyl (**19**) and 4-Br (**20**) benzyloxy derivatives, respectively. Both of these compounds showed enhanced inhibitory activities compared to **10a**, confirming the previous conclusion. Further optimization of the substituent on the quinoline ring, or even replacement of the ring with another heterocycle, merits further effort with the aim of obtaining simplified hybrids as new MTDLs for AD therapy.

Table 2
V_{max} and K_m values for **10f** and **12g** in kinetic studies. Data are shown as mean ± SEM of three independent experiments.

V_{max} and K_m at different concentrations of **10f**			
Concentration (μM)	V_{max} (μM 7 min^{-1})	K_m (μM 7 min^{-1})	R^2
0	0.32 ± 0.03	258.9 ± 72.1	0.93
0.1	0.31 ± 0.02	280.2 ± 60.9	0.96
1	0.26 ± 0.01	241.3 ± 40.0	0.98
5	0.24 ± 0.01	238.5 ± 27.5	0.99
10	0.23 ± 0.01	270.2 ± 39.2	0.98
V_{max} and K_m at different concentrations of **12g**			
Concentration (μM)	V_{max} (μM 7 min^{-1})	K_m (μM 7 min^{-1})	R^2
0	0.53 ± 0.04	263.9 ± 47.0	0.98
0.1	0.52 ± 0.10	313.6 ± 132.8	0.91
1	0.44 ± 0.03	289.3 ± 39.0	0.99
5	0.38 ± 0.03	254.0 ± 46.4	0.98
10	0.33 ± 0.03	286.0 ± 64.1	0.97

2.2.2. Kinetic studies of AChE and BChE inhibition

To determine the nature of the kinetics of AChE and BChE inhibition, the most active compounds toward AChE (**10f**) and BChE (**12g**) were selected for kinetic studies using Lineweaver–Burk plots [17]. Graphical analyses of the steady-state inhibition data for **10f** and **12g** are shown in Fig. 2 A, B. According to the results, increasing concentrations of the compounds (0.1, 1, 5, and 10 μM) resulted in generally stable V_{max} values and increased K_m, indicating a competitive type of inhibition for both **10f** and **12g**. The values of V_{max} and K_m at different concentrations of **10f** and **12g** are shown in Table 2.

2.2.3. Hepatotoxicity study in vitro

Compounds **10f** and **12g** showed good activities in ChE inhibition. The hepatotoxicities of these two compounds were further evaluated through MTT assays of the HepG2 cell line (Fig. 3) [18]. Cells were incubated with **10f** or **12g** at 1, 2.5, 5, and 10 μM, respectively, for 24 h. Concentration-dependent decreases in cell viability were observed for tacrine, **10f**, and **12g**. However, the cell viability with **12g** (93.0%) was higher than that with tacrine (87.9%) at 10 μM. This suggested that **12g**

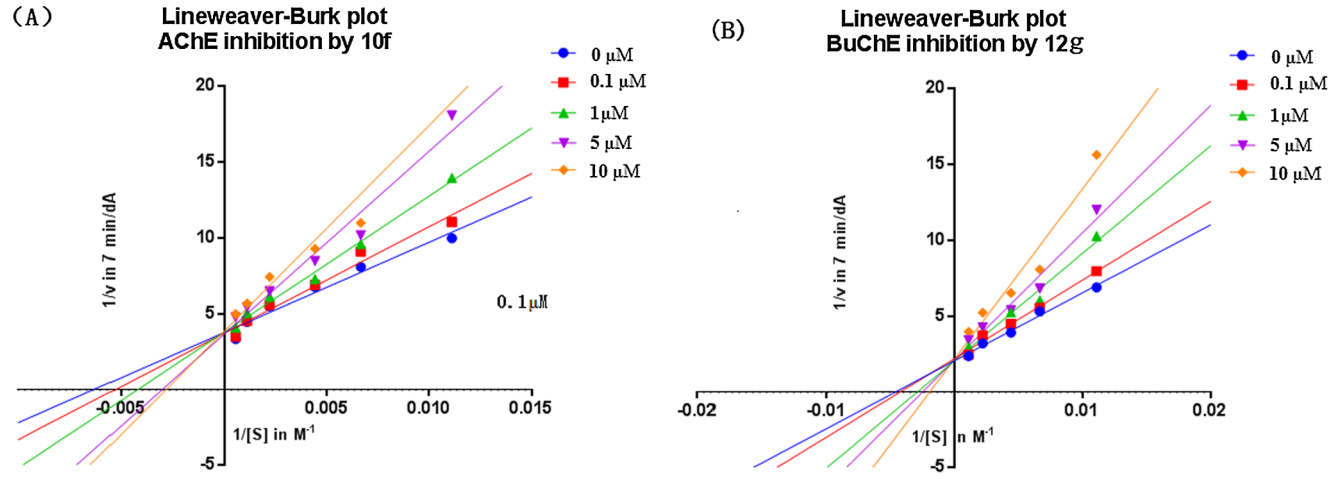

Fig. 2. (A) Lineweaver–Burk plot for the inhibition of eeAChE by compound **10f** at different substrate concentrations. (B) Lineweaver–Burk plot for the inhibition of eqBChE by compound **12g** at different substrate concentrations.

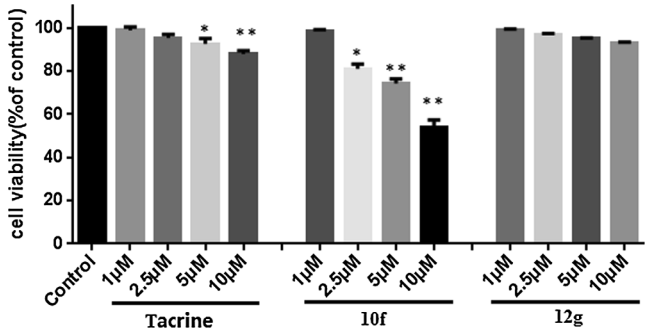

Fig. 3. *In vitro* hepatotoxicities of **10f** and **12g** towards the HepG2 cell line. Data are expressed as the mean ± SD ($n = 3$). *p < 0.05, **p < 0.01, compared with a control group.

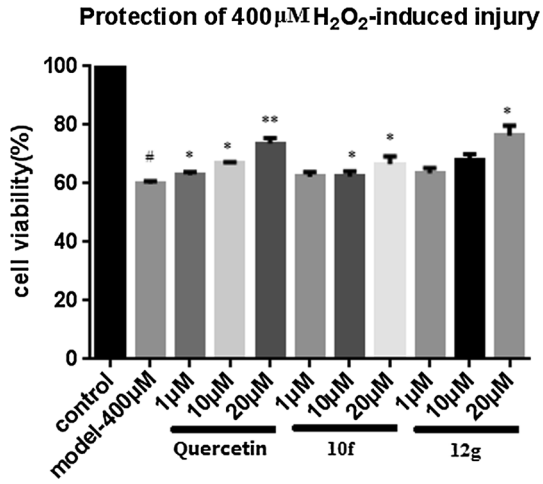

Fig. 4. Protective effects of **10f** and **12g** against H_2O_2-induced cell death in PC-12 cells. Data are expressed as the mean ± SD ($n = 3$). p# < 0.001 compared to a control, p* < 0.05, p** < 0.01 compared to H_2O_2-treated cells.

had a lower hepatotoxicity profile with respect to tacrine. Conversely, the cell viabilities with **10f** (98.6%, 81.0%, 74.3%, and 53.7%) were lower than those with tacrine (98.9%, 95.2%, 92.6%, and 87.9%) under the same conditions, indicating a higher hepatotoxicity of **10f** compared to tacrine.

2.2.4. Neuroprotective effect against H_2O_2-induced cell death in PC12 neurons

The PC12 cell line is a useful model for assessing neuronal differentiation and other neurobiological studies. Hence, we evaluated the neuroprotective activities of **10f** and **12g** against H_2O_2-induced cell damage. Treatment with 400 μM H_2O_2 for 24 h caused over 45% death of PC12 cells compared with a control group (Fig. 4). Quercetine was used as a positive control in the neuroprotective activity assay. When pretreated with **10f** and **12g** for 24 h, the mortality rate of PC-12 cells exposed to H_2O_2 was attenuated. This protective effect showed a dose dependency for both compounds. **10f** showed a better cytoprotective effect (cell viability = 74% at a concentration of 20 μM) than **12g**.

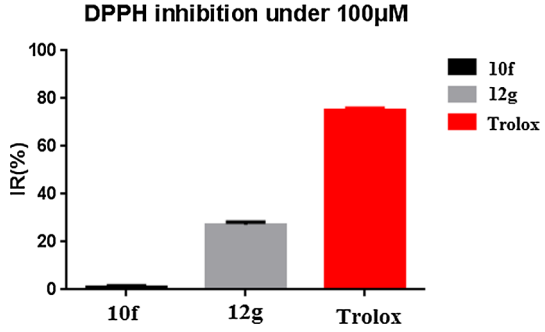

Fig. 5. Inhibitory activities of **10f** and **12g** in DPPH assay.

2.2.5. 1,1-Diphenyl-2-picrylhydrazyl (DPPH) radical scavenging activity

Compounds **10f** and **12g** were further evaluated for their antioxidant activities by using the 1,1-diphenyl-2-picrylhydrazyl (DPPH) radical scavenging method. Trolox was used as the reference compound [19]. **12g** showed a better inhibitory rate than **10f**. The inhibition rate with **12g** was 27% at 100 μM, at which **10f** showed no discernible antioxidant activity (Fig. 5).

2.2.6. Inhibition of self-induced $A\beta_{1-42}$ aggregation

Compounds **10f** and **12g** were evaluated for their inhibitory capacities on self-induced $A\beta_{1-42}$ aggregation based on a thioflavin *T*-based fluorimetric assay. Neither of the tested compounds showed any inhibition activity at concentrations below 33 μM.

2.2.7. Docking studies

Docking studies were performed to identify possible interactions between the compounds and enzyme active sites. Again, **10f** and **12 g** were selected as representative compounds. As shown in Fig. 6A, 10f simultaneously occupies the CAS and PAS of AChE. The quinoline core is located at the CAS through two π-π stacking interactions with Trp86 and Tyr124, respectively. The N atom of the quinoline ring interacts with Ser125 through a hydrogen bond. The phenyl core of the ferulic acid moiety is involved in π-π stacking interaction with Trp286 in the PAS. The benzyloxyl moiety interacts with Leu289 through a π-alkyl contact, and with Ser293 through van der Waals forces. The ethylenediamine linker shows van der Waals interactions with Tyr341 and Asp72.

Molecular docking of **12g** in the active site of BChE is shown in Fig. 6B. The quinoline core interacts with Trp82 through a π-π stacking contact. The N atom of the quinoline ring interacts with Asp70 through a salt bridge. The phenyl ring of the cinnamic acid moiety is engaged in π-alkyl interactions with Gly116. The carbonyl group of the cinnamic acid moiety forms a hydrogen bond with the side chain of His438. The fluorine atom forms a halogen bond with Ser287.

The active site cavity of BChE is broader and larger than that of AChE. The active site cavity of AChE is narrow and long [14,20–21]. **12g** adopts a U-shaped conformation, which is obviously different from the linear conformation of **10f**. It is possible that the U-shaped conformation of **12g** can better occupy the active site of BChE, leading to its selective BChE inhibitory effect.

To explain the effect of the linkers on the ChE inhibitory activities, molecular docking was performed to predict the binding arrangement and to calculate the binding scores of representative compounds **12a** and **14**. As shown in Fig. 7B, 14 occupies the CAS and PAS of AChE. The quinoline core is located at the CAS through three π-π stacking interactions with Trp86 and Tyr124. The N atom of the quinoline ring interacts with Ser125 through a hydrogen bond. The phenyl core of the cinnamic acid moiety is engaged in a π-π stacking interaction with Trp286 in the PAS. When the linker was extended from a two-carbon to a four-carbon chain, the differences compared to **12a** were that the carbonyl group of the cinnamic acid moiety formed a hydrogen bond with the side chain of Phe295, and the N atom of the quinoline ring interacted with Ser125 through a hydrogen bond. The extra hydrogen bonds increase the binding energy of compound **14** (CDOCKER ENERGY = –44.0066 kcal/mol) compared to compound **12a** (CDOCKER ENERGY = –39.9426 kcal/mol). Increasing chain length may be beneficial for increasing the interaction with key amino acids and better occupying the active pocket, thereby enhancing the activity.

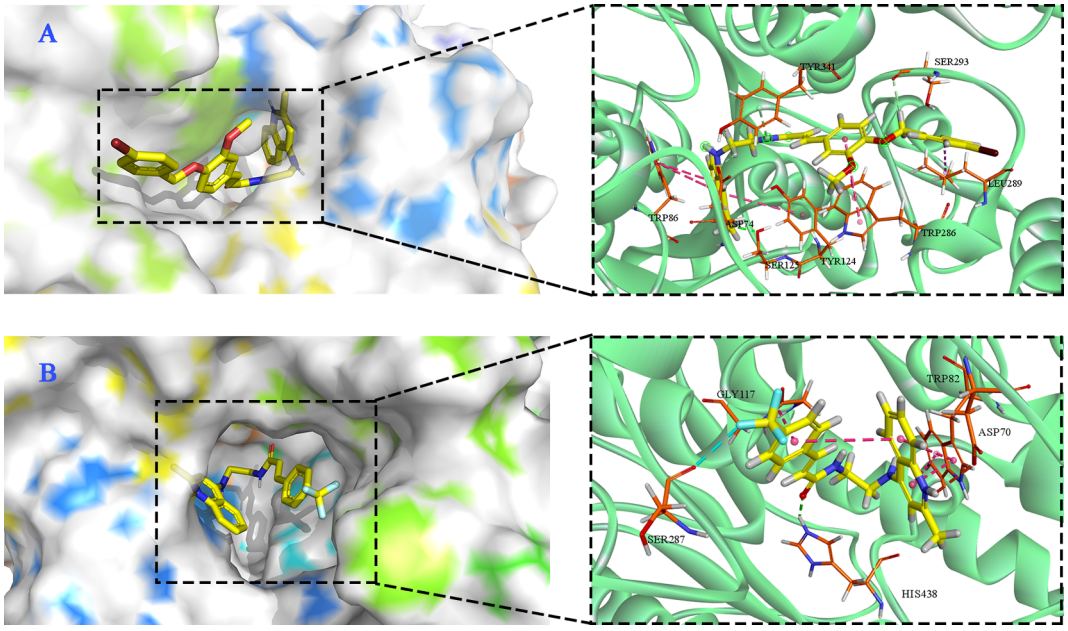

Fig. 6. (A) The AChE active site cavity (left) and an interaction map (right) displaying the binding and interactions of compound **10f**. (B) The BChE active site cavity (left) and interaction map (right) displaying the binding and interactions of compound **12g**. Color coding: green: hydrogen bond; purple: π–π stacking; red: *T*-shaped π–π interaction; orange: salt bridge; blue: halogen bond. (For interpretation of the references to colour in this figure legend, the reader is referred to the web version of this article.)

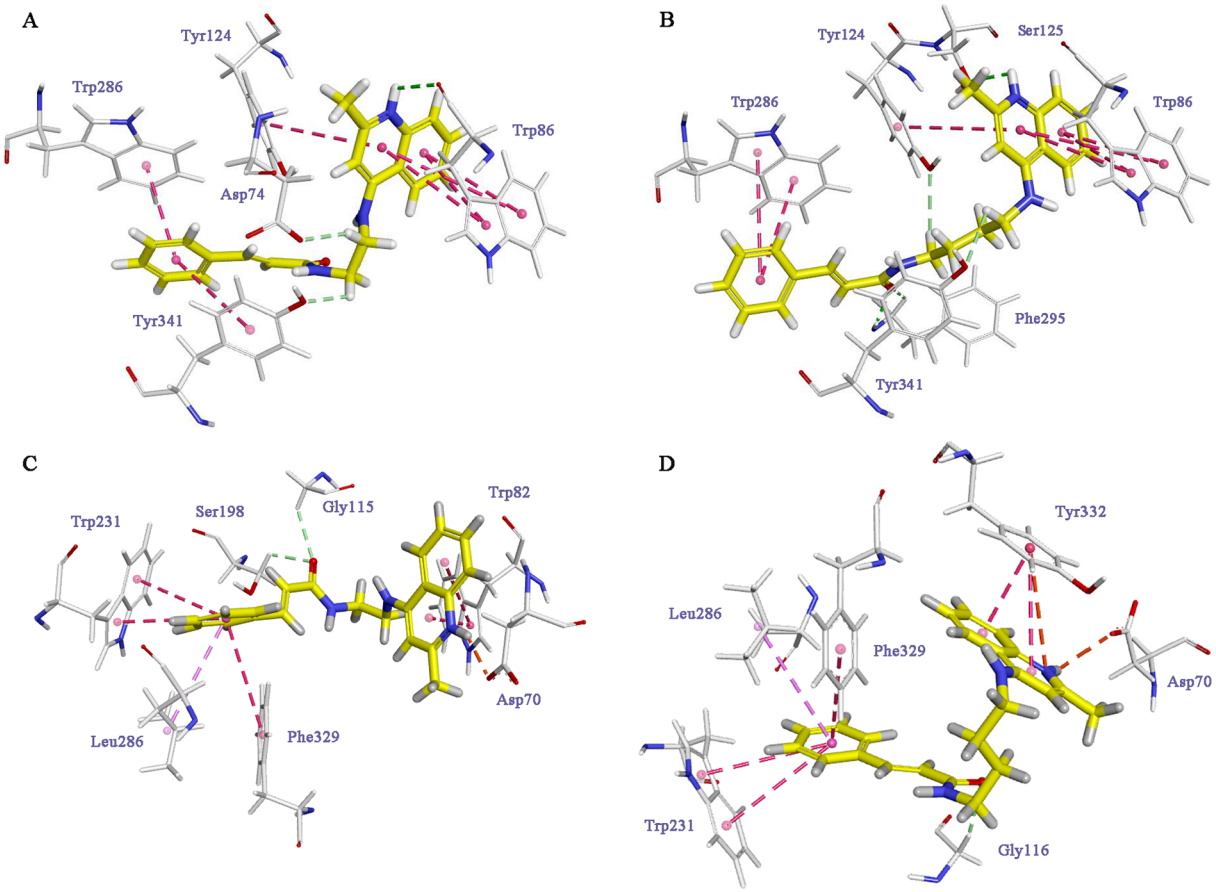

Fig. 7. Binding mode predictions of **12a** (A) and **14** (B) with huAChE (PDB id: 4EY7), and **12a** (C) and **14** (D) with huBChE (PDB id: 4TPK). Compounds are shown in a stick representation and colored yellow. Key residues are shown in a thin stick representation and colored white. Intermolecular interactions are shown as dashed lines of different colors according to their type: light-green, hydrophobic contact; pink, π–π stacking; purple, π–alkyl contact. (For interpretation of the references to colour in this figure legend, the reader is referred to the web version of this article.)

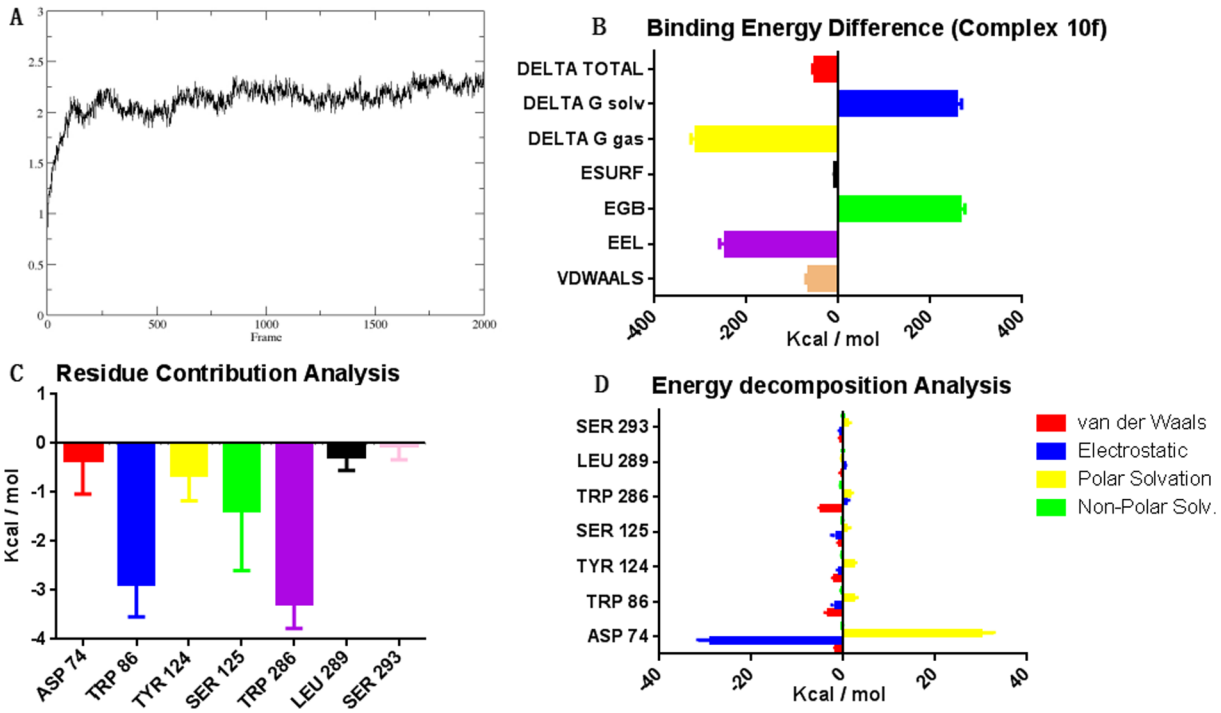

Fig. 8. MD results for **10f** and AChE. (A) RMSD plot for the backbone atoms and **10f** during a 50 ns MD simulation. (B) Binding energy differences of complex **10f** and AChE: delta total, total binding free energy; DELTA G solv, total solvation free energy; DELTA G gas, total gas-phase free energy; ESURF, nonpolar solvation energy; EGB, polar solvation energy; EEL, electrostatic energy; VDWAALS, van der Waals energy. (C) Contribution analysis of potential hot residues. (D) Energy decomposition analysis of potential hot residues. All energies are expressed in kcal/mol.

The binding mode of compound **12a** with BChE is shown in Fig. 7C. The quinoline core is located at the CAS forming two π-π stacking interactions with Trp82. The N atom of the quinoline ring interacts with Asp70 through a salt bridge. This may explain the better inhibitory activity of compound **12a** on BChE than that on AChE. The phenyl core of the cinnamic acid moiety in the PAS is engaged in π-π stacking interactions with Trp231 and Phe329. As shown in Fig. 7D, the quinoline core of compound **14** forms π-π stacking and salt bridge interactions with Tyr332, instead of Trp82 in the case of compound **12a**. The extra salt bridge is beneficial for increasing the binding energy of compound **14** (CDOCKER ENERGY = –45.2775 kcal/mol) compared to compound **12a** (CDOCKER ENERGY = –38.6528 kcal/mol), which may explain the drastically increased inhibitory activity of compound **14** towards BChE.

2.2.8. Molecular dynamics (MD) simulations

After 50 ns MD simulations, the MM/GBSA method was used to calculate the binding free energies and to gain information on the different components of the interaction energies that contribute to compounds **10f** and **12g** binding with AChE and BChE, respectively. Detailed results are shown in Figs. 8 and 9. Fig. 8A and Fig. 9A show the RMSDs of the systems during MD simulations. The RMSDs of ligands after the MD and docking vary within 0.75 Å, implying stable binding of the compounds. Fig. 8B and 9B indicate that electrostatic energy (EEL) and van der Waals energy (VDWAALS) are both vital in the bindings of **10f** and **12g** to AChE and BChE, respectively. Nonpolar solvation energy (ESURF) also contributes to their binding (–7.30 kcal/mol for **10f**–AChE and –5.63 kcal/mol for **12g**–BChE). Meanwhile, polar solvation energy (EGB) is not favorable for the binding of these compounds. The binding free energy for compound **10f**–AChE is higher than that for compound **12 g**–BChE, consistent with our bio-assay results (Table 1).

To identify the key residues contributing to binding affinity, we also conducted an energy decomposition analysis. As shown in Fig. 8C, D and Fig. 9C, D, the hot residues for **10f**–AChE binding are Asp74, Trp86, Tyr124, Ser125, and Trp286, while those for **12g**–BChE binding are Trp82, Gly116, Tyr332, and His438. This information provides a theoretical basis for further lead optimization.

3. Conclusions

In summary, in the present studies, a series of quinoline-ferulic acid and quinoline-cinnamic acid hybrids has been designed and synthesized as MTDLs for the treatment of AD. *In vitro* assays proved that most of the compounds effectively inhibited ChEs in the micromolar range. The detailed mechanisms of the AChE–**10f** and BChE–**12g** interactions at the atomic level were investigated through kinetic experiments, molecular docking, and molecular dynamics simulations. Kinetic studies indicated **10f** (IC_{50} = 0.62 ± 0.17 μM) and **12 g** (IC_{50} = 0.93 ± 0.40 μM) to be competitive inhibitors. Cell toxicity assays using HepG2 cells showed that compound **12g** has a lower hepatotoxicity profile with respect to tacrine. **10f** and **12g** exhibited cytoprotective effects against H_2O_2-induced cell damage. **12g** also showed antioxidant activity according to a DPPH assay. It is noteworthy that when using compounds with longer linkers, such as **14** with a three-carbon linker, AChE inhibitory activity was maintained, but with much improved BChE inhibition, leading to enhanced targeted selectivity towards BChE. We infer that the more flexible chain may lead to a better induced-fit recognition between the compound and BChE. Additionally, as BChE has a broader binding site compared to AChE, a longer linker can provide more intermolecular contacts such as van der Waals interactions. The results may a provide new strategy for designing selective BChE inhibitors.

This study has identified a quinoline-based scaffold for the further design of new MTDLs against AD. The SAR results, especially the tolerance to modification of the quinoline core, suggest that further optimization of the substituent thereon, or even replacement of the ring with another heterocycle, merits further study.

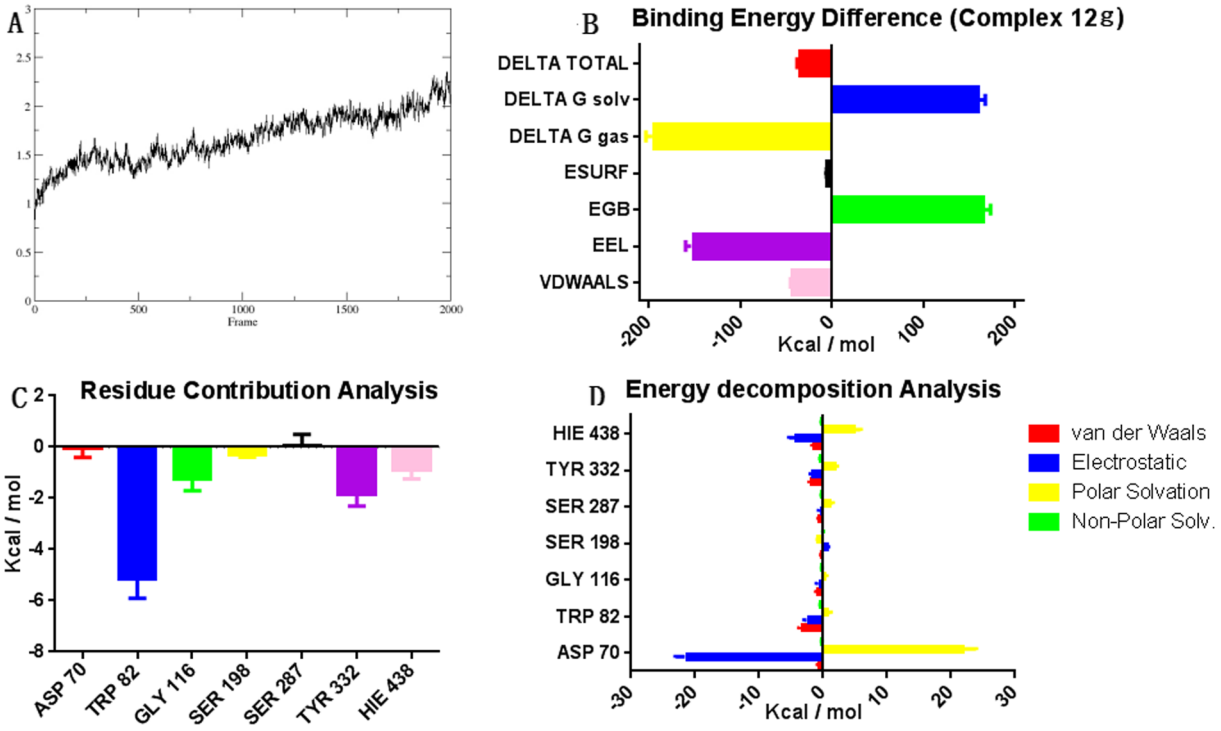

Fig. 9. MD results for **12g** and BChE. (A) RMSD plot for the backbone atoms and **12g** during a 50 ns MD simulation. (B) Binding energy differences of complex **12g** and BChE: delta total, total binding free energy; DELTA G solv, total solvation free energy; DELTA G gas, total gas-phase free energy; ESURF, nonpolar solvation energy; EGB, polar solvation energy; EEL, electrostatic energy; VDWAALS, van der Waals energy. (C) Contribution analysis of potential hot residues. (D) Energy decomposition analysis of potential hot residues. All energies are expressed in kcal/mol.

4. Experimental section

4.1. Chemistry

All the chemicals were purchased from commercial companies and used without purification. All reactions were monitored by analytical thin layer chromatography (TLC) on silica gel 60 F254 precoated plates (purchased from Qingdao Haiyang Inc. China). Visualization was achieved using UV light (254 nm and 365 nm). Flash column chromatography was performed with silica gel (200–300 mesh) purchased from Qingdao Haiyang Chemical Co.Ltd. Melting points were determined using a Mel - TEMP II melting point apparatus. ^{1}H NMR and ^{13}C NMR spectra were recorded on a Bruker Avance (300 MHz for ^{1}H, 500 MHz for ^{13}C, Billerica, MA) at 300 K dissolved in deuterated dimethyl sulfoxide (DMSO-d_6) or deuterated chloroform ($CDCl_3$) with tetramethylsilane (TMS) as an internal standard. Tetramethylsilane (TMS) was used as internal standard. All chemical shifts are reported in parts per million (ppm), relative to the internal standard. The following abbreviations are used to indicate the multiplicities of the respective signals: s - singlet; s - broad singlet; d - doublet; dd - doublet of doublets; t - triplet and m - multiplet. High-resolution mass spectrometry (HRMS) was performed on a Mariner Mass Spectrum (ESI) or an LC/MSD TOF HR-MS Spectrum.

4.1.1. Synthesis of 2-methylquinolin-4-ol (3) [22]

Polyphosphoric acid (15.2 g) was added to a solution of aniline (2.0 g, 21.4 mmol) and ethyl acetoacetate (2.8 g, 21.4 mmol). The reaction mixture was stirred at 130 °C for 3 h. The reaction was monitored by TLC. The reaction mixture was poured into ice water (100 mL) slowly with vigorous stirring. Then the pH value was adjusted to 7 with aqueous NaOH. The precipitated solid was filtered and washed thoroughly with petroleum ether to afford compound **3** as a yellow solid with a yield of 56.0%. ^{1}H NMR (300 MHz, $CDCl_3$): δ 11.55 (s, 1H), 8.37 (d, J = 8.5 Hz, 1H), 7.61 (d, J = 7.0 Hz, 2H), 7.35 (s, 1H), 6.22 (s, 1H), 2.47 (s, 3H). ^{13}C NMR (126 MHz, DMSO-d_6): δ 177.17, 150.11, 140.58, 131.88, 125.23, 124.95, 123.13, 118.21, 108.84, 19.93.

4.1.2. Synthesis of 4-chloro-2-methylquinoline (4)

A mixture of **3** (1.0 g, 6.28 mmol) and $POCl_3$ (12.0 mL) was heated at 120 °C for 4 h. The reaction was monitored by using TLC. After completion of the reaction, excess of $POCl_3$ was distilled off. The residue was stirred with ice water for 10 min, and then the pH value was adjusted to 7 with aqueous NaOH. The compound was collected by filtration and washed with water. The crude product was purified by using flash column chromatography with CH_2Cl_2/methanol (50: 1) elution to afford the white solid compound **4** in 54.0% yield. ^{1}H NMR (300 MHz, $CDCl_3$): δ 8.14 (d, J = 8.3 Hz, 1H), 8.01 (d, J = 8.5 Hz, 1H), 7.71 (t, J = 7.7 Hz, 1H), 7.54 (t, J = 7.6 Hz, 1H), 7.35 (s, 1H), 2.70 (s, 3H).

4.1.3. General procedure for the synthesis of the intermediates 5a-5c

A mixture of **4** (1.0 g, 5.63 mmol) and ethylenediamine or 1,3-propanediamine or 1,4-diaminobutane (1.35, 22.5 mmol) and phenol (1.0 g) and sodium iodide (catalytic amount) were heated at 120 °C for 10 h. The reaction was monitored by using TLC. After completion of the reaction, the resulting mixture was quenched by the addition of water. The aqueous phase was extracted with CH_2Cl_2 (3 × 15 mL). The CH_2Cl_2 layer was then washed with brine and dried over anhydrous Na_2SO_4. After concentration, the crude product was purified by silica gel column chromatograph (CH_2Cl_2/methanol = 50:1) to give intermediates **5a-5c** as a brown oil [16].

4.1.4. General procedure for the synthesis of benzyl (E)-3–(4-(benzyloxy)-3-methoxyphenyl)acrylate (8a-8h)

Compound **6** (1.0 g, 5.15 mmol) and K_2CO_3 (2.85 g, 20.6 mmol) were added to 10 mL of DMF and then stirred at room temperature for 20 min. Compounds **7a-7h** were added dropwisely to the above mixture solution. The reaction was stirred at 85 °C for 5 h and was monitored by

TLC. After completion of the reaction, the reaction mixture was quenched by water. The precipitate was filtrated and the filter cake was washed using water to give the crude product which could be used in the next step without further purification [16].

*4.1.5. General procedure for the synthesis of (E)-3–(4-(benzyloxy)-3-methoxyphenyl)acrylic acid (**9a-9h**)*

To a mixture solution of 2 N × NaOH (30 mL) and MeOH (30 mL) compounds **8a-8h** were added. The reaction mixture was heated to reflux for 3 h. Then, MeOH in the solution was removed and the pH was adjusted to around 2 by adding concentrated HCl. The precipitate was filtrated, washed with cold water, and dried over an infrared lamp to get compounds (**9a-9h**) [16].

*4.1.6. General procedure for the synthesis of (E)-3-(4-(benzyloxy)-3-methoxyphenyl)-N-(2-((2-methylquinolin-4-yl)amino)ethyl)acrylamide (**10a-10h**)*

Compounds (**9a-9 h**) (1.49 mmol) and PyBOP (0.93 g, 1.79 mmol) and DIPEA (0.38 g, 2.98 mmol) were added to 10 mL of DMF and stirred at room temperature for 20 min. Then, compound **5a** (0.3 g, 1.49 mmol) was added and stirred at room temperature for 4 h. After completion of the reaction, the reaction mixture was quenched with water. The aqueous phase was extracted with CH_2Cl_2 (3 × 15 mL). The CH_2Cl_2 layer was then washed with brine and dried over anhydrous Na_2SO_4. After concentration, the crude product was purified by silica gel column chromatograph (CH_2Cl_2/methanol = 80:1) to give compound (**10a-10h**).

*4.1.6.1. (E)-3-(4-(benzyloxy)-3-methoxyphenyl)-N-(2-((2-methylquinolin-4-yl)amino)ethyl)acrylamide (**10a**)*. White solid, yield: 53%, m.p. 121–123 °C. ^{1}H NMR (300 MHz, DMSO-d_6): δ 9.08 (s, 1H), 8.59 (s, 1H), 8.53 (d, J = 8.4 Hz, 1H), 7.95 (d, J = 7.7 Hz, 1H), 7.83 (t, J = 7.3 Hz, 1H), 7.58 (m, 1H), 7.46–7.41 (m, 3H), 7.39 (m, J = 1.7 Hz, 2H), 7.35 (m, J = 5.5 Hz, 1H), 7.18 (d, J = 1.5 Hz, 1H), 7.12–7.01 (m, 2H), 6.79 (s, 1H), 6.57 (d, J = 15.8 Hz, 1H), 5.11 (s, 2H), 3.80 (s, 3H), 3.60 (t, 2H), 3.54 (t, J = 5.5 Hz, 2H), 2.62 (s, 3H). ^{13}C NMR (126 MHz, DMSO-d_6): δ 166.59, 155.43, 154.38, 149.63, 149.59, 139.48, 138.71, 137.28, 133.42, 128.89, 128.38, 128.30, 126.33, 123.60, 121.71, 120.27, 120.14, 116.24, 113.78, 110.85, 98.85, 70.27, 55.98, 43.14, 37.92, 20.50. HRMS (ESI) m/z calcd. for $C_{29}H_{29}N_3O_3$ $[M+H]^+$ 468.2287, found 468.2283.

*4.1.6.2. (E)-3-(3-methoxy-4-((4-methylbenzyl)oxy)phenyl)-N-(2-((2-methylquinolin-4-yl)amino)ethyl)acrylamide (**10b**)*. White solid, yield: 30%, m.p. 167–169 °C. ^{1}H NMR (300 MHz, DMSO-d_6): δ 8.30 (s, 1H), 8.11 (d, J = 7.8 Hz, 1H), 7.75–7.67 (m, 1H), 7.62–7.52 (m, 1H), 7.45 (s, 1H), 7.40 (s, 1H), 7.37 (s, 1H), 7.34 (s, 1H), 7.32 (s, 1H), 7.27 (s, 1H), 7.22–7.20 (m, 1H), 7.19 (s, 1H), 7.07 (m, J = 12.8, 5.0 Hz, 2H), 6.49 (s, 1H), 5.07 (s, 2H), 3.80 (s, 3H), 3.49 (m, 2H), 3.41 (m, J = 5.4 Hz, 2H), 2.48 (s, 3H), 2.31 (s, 3H). ^{13}C NMR (126 MHz, DMSO-d_6): δ 166.54, 158.87, 150.68, 149.68, 149.62, 139.42, 137.62, 134.27, 129.43, 128.38, 123.73, 121.80, 121.74, 120.25, 117.81, 113.86, 110.82, 98.55, 70.20, 55.97, 42.99, 38.12, 25.43, 21.25. HRMS (ESI) m/z calcd. for $C_{30}H_{31}N_3O_3$ $[M+H]^+$ 482.2443, found 482.2444.

*4.1.6.3. (E)-3-(3-methoxy-4-((4-methoxybenzyl)oxy)phenyl)-N-(2-((2-methylquinolin-4-yl)amino)ethyl)acrylamide (**10c**)*. White solid, yield: 72%, m.p. 211–213 °C. ^{1}H NMR (300 MHz, DMSO-d_6): δ 9.24 (s, 1H), 8.56–8.35 (m, 2H), 7.91 (m, J = 5.6 Hz, 2H), 7.66 (m, J = 2.5 Hz, 1H), 7.43–7.28 (m, 2H), 7.17 (s, 1H), 7.08 (m, 3H), 6.95 (m, J = 8.7 Hz, 2H), 6.87 (s, 1H), 6.52 (d, J = 15.8 Hz, 2H), 5.03 (s, 2H), 3.78 (s,3H), 3.76 (s, 3H), 3.64 (t, J = 5.6 Hz, 2H), 3.53 (t, J = 5.8 Hz, 2H), 2.64 (s, 3H). ^{13}C NMR (126 MHz, DMSO-d_6): δ 166.64, 159.53, 155.50, 154.40, 149.72, 149.68, 139.56, 133.51, 130.12, 129.14, 128.20, 126.40, 123.50, 121.75, 120.04, 116.24, 114.27, 113.85, 110.84, 98.88, 70.09, 55.97, 55.57, 43.24, 37.91, 20.56. HRMS (ESI) m/z calcd. for $C_{30}H_{31}N_3O4$ $[M+H]^+$ 498.2393, found 498.2396.

*4.1.6.4. (E)-3-(4-((4-fluorobenzyl)oxy)-3-methoxyphenyl)-N-(2-((2-methylquinolin-4-yl)amino)ethyl)acrylamide (**10d**)*. White solid, yield: 48%, m.p. 215–217 °C. ^{1}H NMR (300 MHz, DMSO-d_6): δ 9.10 (s, 1H), 8.47 (s, 1H), 8.15 (s, 1H), 7.90 (s, 1H), 7.64 (s, 1H), 7.50 (m, 3H), 7.21 (m, J = 12.1 Hz, 4H), 7.08 (s, 2H), 6.84 (s, 1H), 6.53 (d, J = 15.0 Hz, 1H), 5.10 (s, 2H), 3.81 (s, 3H), 3.61 (s, 2H), 3.53 (s, 2H), 2.63 (s, 3H). ^{13}C NMR (126 MHz, DMSO-d_6): δ 166.60, 165.89, 163.24, 161.30, 154.70, 149.66, 149.48, 139.49, 133.55, 130.57, 130.51, 128.43, 126.20, 123.42, 121.70, 120.59, 120.19, 116.35, 115.80, 115.63, 113.89, 110.87, 98.84, 69.58, 55.98, 43.18, 37.92, 20.88. HRMS (ESI) m/z calcd. for $C_{29}H_{28}FN_3O_3$ $[M+H]^+$ 486.2193, found 486.2193.

*4.1.6.5. (E)-3-(4-((4-chlorobenzyl)oxy)-3-methoxyphenyl)-N-(2-((2-methylquinolin-4-yl)amino)ethyl)acrylamide (**10e**)*. White solid, yield: 63%, m.p. 210–213 °C. ^{1}H NMR (300 MHz, DMSO-d_6): δ 8.31 (s, 1H), 8.12 (d, J = 8.0 Hz, 1H), 7.71 (dd, J_1 = 8.4, J_2 = 1.1 Hz, 1H), 7.63–7.55 (m, 1H), 7.47 (m, 4H), 7.39 (m, 2H), 7.31 (s, 1H), 7.21 (d, J = 1.8 Hz, 1H), 7.15–7.02 (m, 2H), 6.59–6.48 (m, 2H), 5.13 (s, 2H), 3.82 (s, 3H), 3.49 (m, 2H), 3.42 (d, 2H), 2.48 (s, 3H). ^{13}C NMR (126 MHz, DMSO-d_6): δ 166.52, 158.90, 150.65, 149.68, 149.32, 147.96, 139.37, 136.40, 132.94, 130.03, 129.37, 128.91, 128.59, 128.33, 123.72, 121.81, 121.68, 120.40, 117.82, 113.94, 110.86, 98.55, 69.44, 55.98, 42.97, 38.12, 25.46. HRMS (ESI) m/z calcd. for $C_{29}H_{28}ClN_3O_3$ $[M+H]^+$ 502.1897, found 502.1899.

*4.1.6.6. (E)-3-(4-((4-bromobenzyl)oxy)-3-methoxyphenyl)-N-(2-((2-methylquinolin-4-yl)amino)ethyl)acrylamide (**10f**)*. White solid, yield: 35%, m.p. 198–200 °C. ^{1}H NMR (300 MHz, DMSO-d_6): δ 8.30 (s, 1H), 8.10 (d, J = 8.3 Hz, 1H), 7.73–7.66 (m, 1H), 7.60 (m, 3H), 7.46–7.33 (m, 4H), 7.21 (d, J = 1.6 Hz, 2H), 7.10 (d, J = 1.6 Hz, 1H), 7.04 (d, J = 8.4 Hz, 1H), 6.57–6.45 (m, 2H), 5.11 (s, 2H), 3.82 (s, 3H), 3.50 (d, J = 5.8 Hz, 2H), 3.41 (d, J = 5.5 Hz, 2H), 2.47 (s, 3H). ^{13}C NMR (126 MHz, DMSO-d_6): δ 166.51, 159.04, 150.48, 149.69, 149.31, 148.27, 139.36, 136.84, 131.83, 130.32, 129.23, 128.62, 123.63, 121.74, 121.67, 121.48, 120.42, 117.87, 113.99, 110.91, 98.54, 69.50, 56.01, 42.97, 38.13, 25.62. HRMS (ESI) m/z calcd. for $C_{29}H_{28}BrN_3O_3$ $[M+H]^+$ 548.1372, found 548.1376.

*4.1.6.7. (E)-3-(3-methoxy-4-((4-(trifluoromethyl)benzyl)oxy)phenyl)-N-(2-((2-methylquinolin-4-yl)amino)ethyl)acrylamide (**10g**)*. White solid, yield: 54%, m.p. 162–165 °C. ^{1}H NMR (500 MHz, DMSO-d_6): δ 13.82 (s, 1H), 9.27 (d, J = 5.3 Hz, 1H), 8.48 (d, J = 8.5 Hz, 1H), 8.43 (s, 1H), 7.91 (s, 2H), 7.78 (d, J = 8.0 Hz, 2H), 7.67 (d, J = 7.7 Hz, 2H), 7.41 (d, J = 15.7 Hz, 1H), 7.21 (s, 1H), 7.11 (d, J = 8.2 Hz, 1H), 7.06 (d, J = 8.4 Hz, 1H), 6.89 (s, 1H), 6.52 (d, J = 15.7 Hz, 1H), 5.26 (s, 2H), 3.83 (s, 3H), 3.64 (d, J = 5.8 Hz, 2H), 3.53 (s, 2H), 2.65 (s, 3H). ^{13}C NMR (126 MHz, DMSO-d_6): δ 165.76, 155.66, 154.30, 139.31, 138.40, 137.78, 133.67, 128.66, 126.50, 126.30, 125.11, 123.58, 120.06, 116.21, 98.89, 42.98, 37.96, 20.43. MS (ESI) m/z = 536.7.

*4.1.6.8. (E)-3-(4-((4-cyanobenzyl)oxy)-3-methoxyphenyl)-N-(2-((2-methylquinolin-4-yl)amino)ethyl)acrylamide (**10h**)*. White solid, yield: 60%, m.p. 193–195 °C. ^{1}H NMR (500 MHz, DMSO-d_6): δ 13.75 (s, 1H), 9.07 (s, 1H), 8.50–8.36 (m, 2H), 7.89 (s, 2H), 7.88 (s, 2H), 7.64 (s, 2H), 7.63 (s, 1H), 7.21 (s, 1H), 7.10 (s, 1H), 7.04 (d, J = 8.4 Hz, 1H), 6.85 (s, 1H), 6.52 (d, J = 15.8 Hz, 1H), 5.25 (s, 2H), 3.83 (s, 3H), 3.62 (d, J = 5.5 Hz, 2H), 3.52 (d, J = 5.9 Hz, 2H), 2.63 (s, 3H). ^{13}C NMR (126 MHz, DMSO-d_6): δ 166.58, 154.95, 149.71, 149.14, 143.20, 139.42, 132.89, 129.96, 128.76, 128.53, 127.89, 126.10, 123.27, 122.30, 121.64, 120.38, 119.21, 116.43, 114.06, 111.04, 111.01, 98.85, 69.36, 56.08, 43.21, 37.93, 21.17. MS (ESI) m/z = 493.7.

*4.1.7. General procedure for the synthesis of N-(2-((2-methylquinolin-4-yl) amino)ethyl)cinnamamide **(12a-12i, 13, 14)***

Compounds **11a-11i** (1.49 mmol) and PyBOP (0.93 g, 1.79 mmol) and DIPEA (0.38 g, 2.98 mmol) were added to 10 mL of DMF and stirred at room temperature for 20 min. Then, compounds **5a-5c** (0.3 g, 1.49 mmol) were added and stirred at room temperature for 4 h. After completion of the reaction, the reaction mixture was quenched with water. The aqueous phase was extracted with CH_2Cl_2 (3 × 15 mL). The CH_2Cl_2 layer was then washed with brine and dried over anhydrous Na_2SO_4. After concentration, the crude product was purified by silica gel column chromatograph (CH_2Cl_2/methanol = 80:1) to give the target compounds (**12a-12i**, **13**, **14**).

*4.1.7.1. N-(2-((2-methylquinolin-4-yl)amino)ethyl)cinnamamide **(12a)***. White solid, yield: 57%, m.p. 110–114 °C. ^{1}H NMR (300 MHz, DMSO-d_6): δ 9.34 (s, 1H), 8.65 (s, 1H), 8.55 (d, J = 8.3 Hz, 1H), 8.03–7.84 (m, 2H), 7.65 (s, 1H), 7.56 (d, J = 6.3 Hz, 2H), 7.50 (s, 1H), 7.46–7.34 (m, 3H), 6.88 (s, 1H), 6.65 (d, J = 15.7 Hz, 1H), 3.66 (d, J = 5.1 Hz, 2H), 3.53 (d, J = 5.5 Hz, 2H), 2.65 (s, 3H). ^{13}C NMR (126 MHz, DMSO-d_6): δ 166.25, 155.64, 154.26, 139.45, 138.39, 135.21, 133.63, 130.03, 129.41, 128.02, 126.48, 123.61, 122.30, 120.03, 116.20, 98.88, 43.05, 37.93, 20.39. HRMS (ESI) m/z calcd. for $C_{21}H_{21}N_3O$ $[M+H]^+$ 332.1763, found 332.1765.

*4.1.7.2. (E)-N-(2-((2-methylquinolin-4-yl)amino)ethyl)-3-(p-tolyl) acrylamide **(12b)***. White solid, yield: 53%, m.p. 100–103 °C. ^{1}H NMR (500 MHz, DMSO-d_6): δ 13.83 (s, 1H), 9.29 (d, J = 5.4 Hz, 1H), 8.51 (d, J = 15.8, 7.2 Hz, 2H), 7.91 (s, 2H), 7.68 (s, 1H), 7.55–7.43 (m, 2H), 7.23 (d, J = 7.9 Hz, 2H), 6.89 (s, 1H), 6.57 (d, J = 15.8 Hz, 1H), 3.65 (d, J = 5.8 Hz, 2H), 3.52 (d, J = 5.9 Hz, 2H), 2.64 (s, 3H), 2.32 (s, 3H). ^{13}C NMR (126 MHz, DMSO-d_6): δ 166.42, 155.67, 154.21, 139.79, 139.39, 138.33, 133.63, 132.46, 129.99, 127.99, 126.48, 123.64, 121.26, 119.96, 116.19, 98.87, 43.09, 37.94, 21.41, 20.33. MS (ESI) m/z = 346.3.

*4.1.7.3. (E)-3-(4-methoxyphenyl)-N-(2-((2-methylquinolin-4-yl)amino) ethyl)acrylamide **(12c)***. White solid, yield: 62%, m.p. 96–99 °C. ^{1}H NMR (500 MHz, DMSO-d_6): δ 8.47 (s, 1H), 8.26 (d, J = 8.3 Hz, 1H), 7.95 (s, 1H), 7.78 (d, J = 8.3 Hz, 1H), 7.68 (s, 1H), 7.52 (d, J = 8.6 Hz, 2H), 7.45 (s, 2H), 6.98 (d, J = 8.6 Hz, 2H), 6.61 (s, 1H), 6.51 (d, J = 15.8 Hz, 1H), 3.79 (s, 3H), 3.49 (s, 4H), 2.52 (s, 3H). ^{13}C NMR (126 MHz, DMSO-d_6): δ 166.55, 160.81, 157.30, 152.34, 139.05, 130.77, 129.59, 127.84, 124.62, 122.53, 119.95, 117.29, 114.84, 98.64, 55.72, 42.96, 38.05, 23.70. MS (ESI) m/z = 362.5.

*4.1.7.4. (E)-3-(4-fluorophenyl)-N-(2-((2-methylquinolin-4-yl)amino) ethyl)acrylamide **(12d)***. White solid, yield: 78%, m.p. 108–110 °C. ^{1}H NMR (300 MHz, DMSO-d_6): δ 9.33 (s, 1H), 8.65–8.44 (m, 2H), 8.06–7.87 (m, 2H), 7.63 (m, 3H), 7.47 (d, J = 15.8 Hz, 1H), 7.25 (t, J = 8.8 Hz, 2H), 6.88 (s, 1H), 6.60 (d, J = 15.9 Hz, 1H), 3.66 (d, J = 5.8 Hz, 2H), 3.54 (d, J = 5.6 Hz, 2H), 2.65 (s, 3H). ^{13}C NMR (126 MHz, DMSO-d_6): δ 166.19, 162.21, 155.68, 154.24, 138.32, 138.27, 133.68, 131.86, 130.23, 130.16, 126.51, 123.60, 122.19, 119.97, 116.47, 116.30, 116.19, 98.88, 43.06, 37.92, 20.37. HRMS (ESI) m/z calcd. for $C_{21}H_{20}FN_3O$ $[M+H]^+$ 350.1668, found 350.1684.

*4.1.7.5. (E)-3-(4-chlorophenyl)-N-(2-((2-methylquinolin-4-yl)amino) ethyl)acrylamide **(12e)***. White solid, yield: 62%, m.p. 158–160 °C. ^{1}H NMR (300 MHz, DMSO-d_6): δ 14.03 (s, 1H), 9.34 (s, 1H), 8.65 (s, 1H), 8.55 (d, J = 8.3 Hz, 1H), 8.06–7.87 (m, 2H), 7.65 (s, 1H), 7.56 (d, J = 6.3 Hz, 2H), 7.46–7.35 (m, 2H), 6.88 (s, 1H), 6.65 (d, J = 15.7 Hz, 1H), 3.66 (d, J = 5.1 Hz, 2H), 3.53 (d, J = 5.5 Hz, 2H), 2.65 (s, 3H). ^{13}C NMR (126 MHz, DMSO-d_6): δ 166.02, 156.10, 153.67, 142.77, 138.04, 134.41, 134.22, 130.36, 129.72, 129.43, 125.38, 123.20, 122.92, 120.79, 116.85, 98.74, 42.92, 38.02, 22.40. MS (ESI) m/z = 366.4.

*4.1.7.6. (E)-3-(4-bromophenyl)-N-(2-((2-methylquinolin-4-yl)amino) ethyl)acrylamide **(12f)***. White solid, yield: 73%, m.p. 175–177 °C. ^{1}H NMR (500 MHz, DMSO-d_6): δ 8.71 (d, J = 5.2 Hz, 1H), 8.18 (d, J = 8.3 Hz, 1H), 7.68 (d, J = 8.3 Hz, 1H), 7.61 (d, J = 8.2 Hz, 2H), 7.53 (d, J = 7.5 Hz, 3H), 7.46 (d, J = 15.8 Hz, 1H), 7.33 (d, J = 7.7 Hz, 2H), 6.77–6.70 (m, 1H), 6.47 (s, 1H), 3.49 (d, J = 5.8 Hz, 2H), 3.42 (d, J = 5.4 Hz, 2H), 2.46 (s, 3H). ^{13}C NMR (126 MHz, DMSO-d_6): δ 165.90, 159.12, 150.39, 148.50, 137.82, 134.68, 132.33, 129.94, 129.10, 128.68, 123.55, 123.49, 123.03, 122.10, 117.98, 98.49, 42.57, 38.15, 25.71. MS (ESI) m/z = 410.6.

*4.1.7.7. (E)-N-(2-((2-methylquinolin-4-yl)amino)ethyl)-3-(4-(trifluoromethyl)phenyl)acrylamide **(12g)***. White solid, yield: 62%, m.p. 158–160 °C. ^{1}H NMR (300 MHz, DMSO-d_6): δ 9.34 (s, 1H), 8.80 (s, 1H), 8.56 (d, J = 8.3 Hz, 1H), 8.26 (d, J = 8.8 Hz, 2H), 7.94 (m, 2H), 7.84 (d, J = 8.8 Hz, 2H), 7.67 (d, J = 8.3, 1.7 Hz, 1H), 7.58 (d, J = 15.8 Hz, 1H), 6.93–6.79 (m, 2H), 3.68 (d, J = 5.9 Hz, 2H), 3.55 (d, J = 5.6 Hz, 2H), 2.65 (s, 3H). ^{13}C NMR (126 MHz, DMSO-d_6): δ 166.58, 155.70, 154.25, 149.67, 139.48, 138.29, 133.73, 128.52, 126.54, 125.84, 123.73, 121.69, 120.25, 120.03, 116.17, 114.07, 110.95, 98.90, 69.36, 56.04, 43.22, 37.87, 20.41. HRMS (ESI) m/z calcd. for $C_{22}H_{20}F_3N_3O$ $[M+H]^+$ 400.1636, found 400.1655.

*4.1.7.8. (E)-N-(2-((2-methylquinolin-4-yl)amino)ethyl)-3-(4-nitrophenyl) acrylamide **(12h)***. White solid, yield: 73%, m.p. 182–185 °C. ^{1}H NMR (300 MHz, DMSO-d_6): δ 9.33 (s, 1H), 8.79 (s, 1H), 8.54 (d, J = 8.5 Hz, 1H), 8.27 (s, 1H), 8.24 (s, 1H), 7.92 (t, J = 3.2 Hz, 2H), 7.85 (s, 1H), 7.82 (s, 1H), 7.66 (m, 1H), 7.57 (d, J = 16.0 Hz, 1H), 6.92–6.80 (m, 2H), 3.67 (d, J = 5.7 Hz, 2H), 3.55 (d, J = 5.5 Hz, 2H), 2.65 (s, 3H). ^{13}C NMR (126 MHz, DMSO-d_6): δ 165.54, 155.71, 154.27, 148.03, 141.82, 138.31, 137.13, 133.71, 129.76, 129.09, 126.57, 124.58, 123.60, 119.98, 116.20, 98.90, 42.95, 38.00, 20.39. HRMS (ESI) m/z calcd. for $C_{21}H_{20}N_4O_3$ $[M+H]^+$ 377.1613, found 377.1616.

*4.1.7.9. (E)-3-(3-cyanophenyl)-N-(2-((2-methylquinolin-4-yl)amino) ethyl)acrylamide **(12i)***. White solid, yield: 68%, m.p. 124–126 °C. ^{1}H NMR (300 MHz, DMSO-d_6): δ 9.35 (s, 1H), 8.69 (s, 1H), 8.55 (d, J = 8.2 Hz, 1H), 8.06 (s, 1H), 7.92 (m, 3H), 7.84 (d, J = 8.0 Hz, 1H), 7.64 (m, 2H), 7.50 (d, J = 15.9 Hz, 1H), 6.91–6.70 (m, 2H), 3.62 (d, J = 20.2 Hz, 2H), 3.54 (d, J = 5.2 Hz, 2H), 2.65 (s, 3H). ^{13}C NMR (126 MHz, DMSO-d_6): δ 165.77, 155.70, 154.27, 138.32, 137.34, 136.59, 133.70, 133.23, 132.23, 131.75, 130.62, 126.52, 124.74, 123.60, 119.99, 118.92, 116.19, 112.57, 98.89, 42.99, 37.96, 20.40. HRMS (ESI) m/z calcd. for $C_{22}H_{20}N_4O$ $[M+H]^+$ 357.1715, found 357.1717.

*4.1.7.10. N-(3-((2-methylquinolin-4-yl)amino)propyl)cinnamamide **(13)***. Yellow solid, yield: 69%, m.p. 107–109 °C. ^{1}H NMR (500 MHz, DMSO-d_6): δ 8.29 (s, 1H), 8.19 (d, J = 8.2 Hz, 1H), 7.70 (d, J = 7.9 Hz, 1H), 7.57 (d, J = 7.3 Hz, 3H), 7.46 (d, J = 15.8 Hz, 1H), 7.41 (d, J = 7.5 Hz, 2H), 7.39–7.34 (m, 2H), 7.21 (s, 1H), 6.67 (d, J = 15.8 Hz, 1H), 6.40 (s, 1H), 3.37–3.29 (m, 4H), 2.47 (s, 3H), 1.91–1.85 (m, 2H). ^{13}C NMR (126 MHz, DMSO-d_6): δ 165.61, 158.77, 150.72, 147.80, 139.06, 135.38, 129.88, 129.39, 128.14, 127.95, 123.68, 122.66, 121.95, 117.88, 98.53, 55.38, 37.13, 28.41, 25.34. HRMS (ESI) m/z calcd. for $C_{22}H_{23}N_3O$ $[M+H]^+$ 346.1919, found 346.1917.

*4.1.7.11. N-(4-((2-methylquinolin-4-yl)amino)butyl)cinnamamide **(14)***. Yellow solid, yield: 74%, m.p. 97–99 °C. ^{1}H NMR (500 MHz, DMSO-d_6): δ 8.19 (d, J = 8.5 Hz, 2H), 7.69 (d, J = 8.3 Hz, 1H), 7.55 (d, J = 7.2 Hz, 3H), 7.44 (d, J = 12.3 Hz, 1H), 7.42–7.39 (m, 2H), 7.36 (m, 2H), 7.15 (s, 1H), 6.65 (d, J = 15.8 Hz, 1H), 6.38 (s, 1H), 3.34–3.24 (m, 4H), 2.46 (s, 3H), 1.77–1.68 (m, 2H), 1.64–1.56 (m, 2H). ^{13}C NMR (126 MHz, DMSO-d_6): δ 165.35, 158.84, 150.72, 138.91, 135.41, 129.83, 129.38, 129.30, 128.24, 127.91, 123.53, 122.78, 122.01, 117.87, 98.48, 42.55, 38.84, 27.36, 25.80, 25.42. HRMS (ESI) m/z

calcd. for $C_{23}H_{25}N_3O$ $[M+H]^+$ 346.1919, found 346.1917.

*4.1.8. Synthesis of the target compounds **18-20***

*4.1.8.1. Synthesis of 4-chloroquinoline **(16)**.* A mixture of **15** (1.0 g, 6.89 mmol) and $POCl_3$ (12 mL) was heated at 120 °C for 4 h. The reaction was monitored by using TLC. After completion of the reaction, excess of $POCl_3$ was distilled off. The residue was stirred with ice water for 10 min, and then the pH value was adjusted to 7 with aqueous NaOH. The compound was collected by filtration and washed with water. The crude product was purified by using flash column chromatography with CH_2Cl_2/methanol (100: 1) elution to afford a white solid compound **16**. ^{1}H NMR (300 MHz, DMSO-d_6): δ 8.85 (d, J = 4.6 Hz, 1H), 8.20 (d, J = 8.4 Hz, 1H), 8.11 (d, J = 8.4 Hz, 1H), 7.88 (t, J = 7.6 Hz, 1H), 7.81–7.72 (m, 2H).

*4.1.8.2. Synthesis of N^1-(quinolin-4-yl)ethane-1,2-diamine **(17)**.* A mixture of **16** (1.0 g, 6.11 mmol) and ethylenediamine (1.47, 24.45 mmol) and phenol (1.0 g) and sodium iodide (catalytic amount) were heated at 120 °C for 10 h. The reaction was monitored by using TLC. After completion of the reaction, the resulting mixture was quenched by the addition of water, the aqueous phase was extracted with CH_2Cl_2 (3 × 15 mL). The CH_2Cl_2 layer was then washed with brine and dried over anhydrous Na_2SO_4. After concentration, the crude product was purified by silica gel column chromatograph (CH_2Cl_2/methanol = 40:1) to give compound **17** as a brown oil. ^{1}H NMR (300 MHz, DMSO-d_6): δ 8.40 (d, J = 5.2 Hz, 1H), 8.25 (d, J = 8.4 Hz, 1H), 7.79 (d, J = 8.3 Hz, 1H), 7.60 (t, J = 7.6 Hz, 1H), 7.41 (t, J = 7.5 Hz, 1H), 7.16 (s, 1H), 6.48 (d, J = 5.2 Hz, 1H), 3.19 (d, J = 0.8 Hz, 2H), 2.87 (t, J = 6.3 Hz, 2H).

4.1.8.3. General synthesis of the target compounds 18–20. Compound **9a**, **9b** or **9f** (1.60 mmol) and PyBOP (1.0 g, 1.92 mmol) and DIPEA (0.41 g, 3.20 mmol) were added to 10 mL of DMF and stirred at room temperature for 20 min. Then, compound **17** (0.3 g, 1.60 mmol) was added and stirred at room temperature for 4 h. After completion of the reaction, the reaction mixture was quenched with water. The aqueous phase was extracted with CH_2Cl_2 (3 × 15 mL). The CH_2Cl_2 layer was then washed with brine and dried over anhydrous Na_2SO_4. After concentration, the crude product was purified by silica gel column chromatograph (CH_2Cl_2/methanol = 80:1) to give the target compounds.

*4.1.8.4. (E)-3-(4-(benzyloxy)-3-methoxyphenyl)-N-(2-(quinolin-4-ylamino)ethyl)acrylamide **(18)**.* White solid, yield: 65%, m.p. 253–255 °C. ^{1}H NMR (300 MHz, DMSO-d_6): δ 8.41 (d, J = 5.3 Hz, 1H), 8.33 (m, 1H), 8.17 (d, J = 7.8 Hz, 1H), 7.81–7.74 (m, 1H), 7.66–7.57 (m, 1H), 7.44 (m, J = 5.2, 2.6 Hz, 4H), 7.40 (s, 2H), 7.35 (m, J = 5.9, 2.1 Hz, 1H), 7.34–7.30 (m, 1H), 7.20 (m, J = 1.6 Hz, 1H), 7.08 (m, 2H), 6.64–6.47 (m, 2H), 5.13 (s, 2H), 3.82 (s, 3H), 3.51 (t, J = 6.0 Hz, 2H), 3.42 (t, J = 5.6 Hz, 2H). ^{13}C NMR (126 MHz, DMSO-d_6): δ 166.52, 151.19, 150.29, 149.67, 149.57, 148.76, 139.41, 137.31, 129.53, 129.19, 128.90, 128.42, 128.38, 128.29, 124.35, 121.97, 121.76, 120.32, 119.26, 113.81, 110.80, 98.61, 70.29, 55.97, 42.98, 38.01. HRMS (ESI) m/z calcd. for $C_{28}H_{27}N_3O_3$ $[M+H]^+$ 454.2130, found 454.2128.

*4.1.8.5. (E)-3-(3-methoxy-4-((4-methylbenzyl)oxy)phenyl)-N-(2-(quinolin-4-ylamino)ethyl)acrylamide **(19)**.* White solid, yield: 65%, m.p. 245–247 °C. ^{1}H NMR (500 MHz, DMSO-d_6): δ 8.43 (d, J = 5.4 Hz, 1H), 8.34 (s, 1H), 8.21 (d, J = 8.3 Hz, 1H), 7.80 (d, J = 8.3 Hz, 1H), 7.64 (t, J = 7.6 Hz, 1H), 7.51 (s, 1H), 7.48–7.40 (m, 2H), 7.33 (d, J = 7.9 Hz, 2H), 7.20 (d, J = 8.2 Hz, 2H), 7.09 (d, J = 1.6 Hz, 1H), 7.05 (d, J = 8.4 Hz, 1H), 6.60 (d, J = 5.5 Hz, 1H), 6.54 (d, J = 15.7 Hz, 1H), 5.07 (s, 2H), 3.80 (s, 3H), 3.50 (d, J = 6.0 Hz, 2H), 3.43 (d, J = 5.7 Hz, 2H), 2.31 (s, 3H). ^{13}C NMR (126 MHz, DMSO-d_6): δ 166.54, 150.88, 150.36, 149.68, 149.62, 147.73, 139.44, 137.62, 134.26, 129.65, 129.43, 128.64, 128.38, 128.35, 124.61, 122.18, 121.76, 120.26, 119.07, 113.84, 110.82, 98.60, 70.21, 55.97, 43.03, 38.01, 21.24. HRMS (ESI) m/z calcd. for $C_{29}H_{29}N_3O_3$ $[M+H]^+$ 468.2287, found 468.2277.

*4.1.8.6. (E)-3-(4-((4-bromobenzyl)oxy)-3-methoxyphenyl)-N-(2-(quinolin-4-ylamino)ethyl)acrylamide **(20)**.* White solid, yield: 67%, m.p. 256–258 °C. ^{1}H NMR (500 MHz, DMSO-d_6): δ 8.43 (d, J = 5.4 Hz, 1H), 8.34 (s, 1H), 8.20 (d, J = 8.4 Hz, 1H), 7.80 (d, J = 8.3 Hz, 1H), 7.67–7.62 (m, 1H), 7.60 (d, J = 8.2 Hz, 2H), 7.50 (s, 1H), 7.45 (d, J = 10.1 Hz, 1H), 7.41 (d, J = 8.1 Hz, 2H), 7.21 (s, 1H), 7.10 (s, 1H), 7.05 (s, 1H), 6.60 (d, J = 5.5 Hz, 1H), 6.54 (d, J = 15.7 Hz, 1H), 5.11 (s, 2H), 3.82 (s, 3H), 3.50 (d, J = 6.0 Hz, 2H), 3.44 (d, J = 5.6 Hz, 2H). ^{13}C NMR (126 MHz, DMSO-d_6): δ 166.52, 150.89, 150.35, 149.69, 149.32, 147.71, 144.18, 139.38, 136.82, 131.82, 130.32, 129.66, 128.62, 124.61, 122.16, 121.70, 121.48, 120.42, 119.06, 113.97, 110.91, 98.60, 69.50, 56.01, 46.00, 43.03, 38.01. HRMS (ESI) m/z calcd. for $C_{28}H_{26}BrN_3O_3$ $[M+H]^+$ 534.1236, found 534.1212.

4.2. AChE and BChE inhibition assay

The inhibitory effects of the target compounds were evaluated followed the method of Ellman *et al* [17]. AChE (EC 3.1.1.7, Type VI-S, from electric eel, C3389) and BChE (EC 3.1.1.8, from equine serum, C0663), 5,5′-dithiobis (2-nitrobenzoic acid) (DTNB, D218200), substrates acetylthiocholine iodide (ATC, A5751) and butyrylthiocholine iodide (BTC, B3253) were obtained from Sigma-Aldrich (St. Louis, MO, USA). Briefly, the assay phosphate buffer solution was prepared as follow: 1) 13.6 g potassium dihydrogen phosphate dissolved in 1 L distilled water; 2) the pH of buffer solution was adjusted to 8.0 ± 0.1 using 10% KOH solution (w/v). For AChE / BChE stock solution, the protein from Sigma was diluted using 0.2 M phosphate buffer (pH 8.0) to prepare 2.5 units per mL. For the preparation of the ATC/BTC ioide solution (0.075 M), they were diluted with distilled water to give the substrate solution. DTNB was diluted with 0.15% (w/v) sodium bicarbonate solution to give 10 μM per mL. The test smaples were firstly dissolved in DMSO to give an initial concentration of 100 μM, which was then diluted using methanol to the target concentration ranging from 10 μM to 1 nM. These samples with different concentrations were used in the subsequent IC_{50} determination.

For measurement, 3 mL of phosphate buffer, 100 μL of AChE/BChE, 100 μL of DTNB, and 100 μL test compound solution was added into a cuvette in order. The enzymatic reaction was started when adding 20 μL of ATC or BTC, and the mixture was immediately stirred. After two minutes, the absorption was measured at 25 °C at 412 nm using a Varioskan Flash 3001 spectrophotometer (from Thermo, USA) as detector. For the control group, 100 μL of methanol was used to replace test compound solution, while a mixture of 80 μL distilled water and 20 μL DTNB solution was used to replace enzyme solution as the blank group. The determination of all the test samples was performed in triplicate. GraphPad Prism 6.0 (GraphPad Software, Inc., La Jolla, CA) was used for data processing. The inhibition curve was fitted by plotting percentage enzyme activity (100% for the reference) versus the logarithm of the concentration of tested compound. The half maximal inhibitory concentration (IC_{50}) value was calculated on the basis of the inhibition curve. The data was calculated and shown in the form of mean ± SEM.

4.3. Kinetic studies of AChE and BChE inhibition

Kinetic studies were performed in the same manner as the determination of ChEs inhibition, while the substrate (ATC/BTC) was used in concentrations of 90, 150, 226, 452 and 904 μM. The concentrations of test compounds were set to 0, 0.1, 1, 5, 10 μM for both **10f** and **12g**. The enzymatic reaction was extended to 7 min for eeAChE

and eqBChE before the determination of the absorption. Vmax and Km values of the Michaelis–Menten kinetics were calculated by nonlinear regression from substrate-velocity curves using GraphPad Prism 6.0. Linear regression was used for fitting the Lineweaver–Burk plots.

4.4. Hepatotoxicity study in vitro

HepG2 cells (human hepatocellular liver carcinoma cell line purchased from Cell Bank of the Chinese Academy of Sciences (Shanghai, China), were cultivated in DMEM supplemented with 10% FBS at 37 °C in a humidified atmosphere containing 5% CO_2. For the determination, cells (6×10^3 cells/well) were seeded in 96-well plate in complete medium. After 24 h, the medium was removed, and cells were exposed to the increasing concentrations of compounds **10f** and **12g** or tacrine (1, 2.5, 5 and 10 μM) in DMEM for further 24 h. Cell survival was measured through MTT assay.

4.5. Neuroprotection assay

PC-12 cells were plated in 96-well plates, raised to a population of 1×10^4 cells per well, and incubated overnight. The assay was initially performed by treating the cells with the test compounds or DMSO for 24 h at 37 °C, and then the cells were further incubated with 400 μM H_2O_2 for another 24 h. After that, 20.0 μL of MTT solution was added into each well of the plate and incubated for 4 h. Then the solution was removed and 150.0 mL of DMSO was added into each well to dissolve the MTT formazan crystals. DMSO was used as a negative control. The absorbance values (OD value) were read at 570 nm by Elx800 Absorbance Microplate Reader (BioTek, Vermont, USA). Results were adjusted considering OD measured in the blank.

4.6. Antioxidant activity in vitro

The antioxidant activities of compounds **10f** and **12g** were evaluated by DPPH free-radical scavenging assay according to the method of Lee et al. with slightly modifications [23]. Briefly, 95 mL of DPPH radical solution (100 μM) was added in a 96-well plate containing 5 mL of different concentrations of test compounds dissolved in DMSO, and incubated for 30 min at 37 °C in the dark. The absorbance of each well was measured at 517 nm using a Varioskan Flash 3001 microplate reader (Thermo, USA).

4.7. Inhibition of self-induced $A\beta_{1-42}$ aggregation

Inhibitory effects of the compounds on self-induced $A\beta_{1-42}$ aggregation were tested through a Thioflavin T (ThT, T3516, Sigma-Aldrich) binding assay [24]. Firstly, aliquots of 2 μL of $A\beta_{1-42}$ (AS-64129–05 Anaspec Inc.) containing 2 mg/mL HFIP (1,1,1,3,3,3-hexafluoro-2-propanol, 52517, Sigma-Aldrich) were stocked in DMSO. Then, they were diluted with 0.215 M sodium phosphate buffer (pH 8.0) to the final concentration of 500 μM. Test compounds were dissolved in DMSO and then prepared at a concentration of 33 μM by the buffer. Resveratrol was used as a positive control. The $A\beta_{1-42}$ and the test sample solutions were incubated in a 96-well plate for 24 h at room temperature. After the incubation, the tested compounds were diluted to a final volume of 150 μL with 50 mM glycine-NaOH buffer (pH 8.5) containing 5 mM ThT. Fluorescence intensity was read (excitation wavelength 450 nm, emission wavelength 485 nm) on a SpectraMax Paradigm Multimode Reader (Molecular Device, Sunnyvale, CA).

The calculation of the inhibitory rate of $A\beta_{1-42}$ self-induced aggregation was performed as the following equation: $(1\text{-}I_{Fi}/I_{Fc}) \times 100\%$. I_{Fi} and I_{Fc} were the fluorescence intensities measured in the presence and absence of inhibitors, respectively, after subtracting the background fluorescence of the 5 mM ThT solution. Each compound was measured in triplicate.

4.8. Molecular docking study

The crystal structures of the hAChE (PDB ID: 4EY7) [25] and hBChE (PDB ID: 4TPK) [26] were derived from the RCSB Protein Data Bank (PDB). Docking studies were carried out using the discovery studio (DS, version 3.0, BIOVIA, San Diego, CA) for compound **10f** and compound **12g**. Two protein structures were preprocessed by "prepare protein" module in DS to give the structures suitable for docking. "Prepare ligands" module in DS was applied for the structural preparation of the test compounds. The native ligand in the crystal structure was used to define the binding site. The binding site was defined as a site sphere (in 10 Å radius) around the original ligands in the co-crystal structures. The docking program CDOCKER encoded in DS 3.0 was applied to identify the potential binding pattern of compound **10f** to the hAChE and compound **12g** to the hBChE. Other CDOCKER parameters were set as default.

4.9. Molecular dynamics (MD) simulations

MD simulations were performed using the PMEMD module in AMBER 16 accelerated by GPU system consist of the NVIDIA CUDA processor [27]. The initial structures of **10f** and **12g** binding in AChE or BChE from molecular docking were used for MD. The proteins were assigned with the AMBER ff99SB force field [28]. The ANTECHAMBER module and the general AMBER force field [29] was applied to the ligands. The systems were solvated in a TIP3P water box in a 9 Å hexahedron. Sodium ions were added with the purpose of neutralization of the systems. To remove possible steric stresses, the systems were minimized for 1000 steps with the steepest descent method, followed by application of conjugate gradients for another 1000 steps. All two systems were linearly heated from 0 to 300 K using a Langevin thermostat and weak restraints of 10 kcal/mol on the protein backbone atoms over 1 ns. Finally, dynamics simulations of 20 ns NPT ensemble at 1 atm and 300 K. After MD simulation, 2000 frames were extracted from the 20 ns of trajectory for CPPTRAJ analysis [30]. The MMGBSA method in the AMBER 16 was used to calculate the binding free energies and energy decomposition [31].

Acknowledgements

We gratefully thank the support from the grants (Nos. 81872728 and 81573281) of National Natural Science Foundation of China, (Nos. BK20191411) of Natural Science Foundation of Jiangsu Province. We thank the support from Double First-Class" initiative Innovation team project of China Pharmaceutical University (Nos. CPU2018GF11 and CPU2018GY34), and Jiangsu Qinglan Project (Yao Chen). Finally, we thank International Science Editing (http://www.internationalscienceediting.com) for editing this manuscript.

Appendix A. Supplementary material

Supplementary data to this article can be found online at https://doi.org/10.1016/j.bioorg.2019.103310.

References

[1] M. Goedert, M.G. Spillantini, A century of Alzheimer's disease, Science 314 (2006) 777–781.
[2] Alzheimer's Disease International. World Alzheimer Report 2015: The global impact of dementia: an analysis of prevalence, incidence, costs and trends. London: Alzheimer's Disease International (ADI); 2015. Available at: https://www. alz.co.uk/research/world-report-2015.
[3] A. Kumar, A. Singh, Ekavali, A review on Alzheimer's disease pathophysiology and its management: an update, Pharmacol. Rep. 67 (2015) 195–203.
[4] C. Berk, G. Paul, M. Sabbagh, Investigational drugs in Alzheimer's disease: current progress, Expert Opin. Invest. Drugs 23 (2014) 837–846.
[5] H. Gocer, A. Akincioglu, S. Goksu, et al., Carbonic anhydrase and acetylcholinesterase inhibitory effects of carbamates and sulfamoylcarbamates, J.

Enzyme Inhib. Med. Chem. 30 (2015) 316–320.
[6] T.H. Ferreiravieira, I.M. Guimaraes, F.R. Silva, et al., Alzheimer's disease: targeting the cholinergic system, Curr. Neuropharmacol. 14 (1) (2016).
[7] S.S. Xie, X.B. Wang, J.Y. Li, et al., Design, synthesis and evaluation of novel tacrine-coumarin hybrids as multifunctional cholinesterase inhibitors against Alzheimer's disease, Eur. J. Med. Chem. 64 (2013) 540–553.
[8] M. Hosoi, K. Hori, K. Konishi, et al., Plasma cholinesterase activity in Alzheimer's disease, Neurodegener. Dis. 15 (2015) 188–190.
[9] C.G. Ballard, N.H. Greig, A.L. Guillozet-Bongaarts, et al., Cholinesterases: roles in the brain during health and disease, Curr. Alzheimer Res. 2 (2005) 307–318.
[10] U. Holzgrabe, P. Kapkova, V. Alptuzun, et al., Targeting acetylcholinesterase to treat neurodegeneration, Expert Opin. Ther. Tar. 11 (2007) 161–179.
[11] N.H. Greig, D.K. Lahiri, K. Sambamurti, Butyrylcholinesterase: an important new target in Alzheimer's disease therapy, Int. Psychogeriatr. 14 (2002) 77–91.
[12] N.H. Greig, T. Utsuki, D.K. Ingram, et al., Selective butyrylcholinesterase inhibition elevates brain acetylcholine, augments learning and lowers Alzheimer β-amyloid peptide in rodent, Proc. Natl. Acad. Sci. U S A 102 (47) (2005) 17213–17218.
[13] E. Giacobini, Cholinergic function and Alzheimer's disease, Int. J. Geriat Psychiatry 18 (2003) S1–S5.
[14] J.T. Zhou, X.Y. Jiang, S.Y. He, et al., Rational design of multi-target-directed ligands: strategies and emerging paradigms, J. Med. Chem. (2019), https://doi.org/10.1021/acs. jmcdchem. 9b00017.
[15] Y. Chen, H. Lin, J. Zhu, et al., Design, synthesis, in vitro and in vivo evaluation of tacrine–cinnamic acid hybrids as multi-target acetyl- and butyrylcholinesterase inhibitors against Alzheimer's disease, RSC Adv. 7 (54) (2017) 33851–33867.
[16] J. Zhu, H. Yang, Y. Chen, et al., Synthesis, pharmacology and molecular docking on multifunctional tacrine-ferulic acid hybrids as cholinesterase inhibitors against Alzheimer's disease, J. Enzyme Inhib. Med. Chem. 33 (1) (2018) 496–506.
[17] G.L. Ellman, K.D. Courtney, V. Andres Jr, R.M. Feather-Stone, A new and rapid colorimetric determination of acetylcholinesterase activity, Biochem. Pharmacol. 7 (1961) 88–95.
[18] L. Pourabdi, M. Khoobi, H. Nadri, et al., Synthesis and structure-activity relationship study of tacrine-based pyrano[2,3-c]pyrazoles targeting AChE/BChE and 15-LOX, Eur. J. Med. Chem. 123 (2016) 298–308 Complete.
[19] S.S. Xie, X.B. Wang, J.Y. Li, et al., Design synthesis and evaluation of novel tacrine-coumarin hybrids as multifunctional cholinesterase inhibitors against Alzheimer's disease, Eur. J. Med. Chem. 64 (2013) 540–553.
[20] J.L. Sussman, M. Harel, F. Frolow, et al., Atomic structure of acetylcholinesterase from Torpedo californica: a prototypic acetylcholine-binding protein, Science 253 (5022) (1991) 872–879.
[21] Bourne Y, Taylor P, Zoran Radi|[cacute, et al. Structural insights into ligand interactions at the acetylcholinesterase peripheral anionic site. Embo Journal, 2014, 22(1):1–12.
[22] Z.Q. Liu, S.T. Zhuo, J.H. Tan, et al., Facile syntheses of disubstituted bis(vinylquinolinium)benzene derivatives as G-quadruplex DNA binders, Tetrahedron 69 (24) (2013) 4922–4932.
[23] S.S. Xie, J.S. Lan, X.B. Wang, et al., Multifunctional tacrine–trolox hybrids for the treatment of Alzheimer's disease with cholinergic, antioxidant, neuroprotective and hepatoprotective properties, Eur. J. Med. Chem. 93 (2015) 42–50.
[24] L.L. Xu, X. Zhang, Z.Y. Jiang, et al., Molecular similarity guided optimization of novel Nrf2 activators with 1,2,4-oxadiazol core, Bioorg. Med. Chem. (2016) S0968089616304011.
[25] J. Cheung, M.J. Rudolph, F. Burshteyn, et al., Structures of human acetylcholinesterase in complex with pharmacologically important ligands, J. Med. Chem. 55 (2012) 10282–10286.
[26] B. Brus, U. Kosak, S. Turk, et al., Discovery, biological evaluation, and crystal structure of a novel nanomolar selective butyrylcholinesterase inhibitor, J. Med. Chem. 57 (2014) 8167–8179.
[27] Case, David & Betz, Robin & Cerutti, D.S. & Cheatham, Thomas & Darden, Thomas & Duke, Robert & Giese, T.J. & Gohlke, H & Götz, Andreas & Homeyer, N & Izadi, Saeed & Janowski, Pawel & Kaus, J & Kovalenko, Andriy & Lee, Tai-Sung & LeGrand, S & Li, P & Lin, C & Luchko, Tyler & Kollman, P.A. (2016). Amber 2016, University of California, San Francisco. 10.13140/RG. 2. 2. 27958. 70729.
[28] V. Hornak, R. Abel, A. Okur, B. Strockbine, A. Roitberg, C. Simmerling, Proteins 65 (2006) 712.
[29] Z. Wei, T. Hou, A. Xuebin Qiao, et al., Parameters for the generalized born model consistent with RESP atomic partial charge assignment protocol, J. Phys. Chem. B 107 (34) (2003) 9071–9078.
[30] D.R. Roe, C.T. Rd, PTRAJ and CPPTRAJ: Software for processing and analysis of molecular dynamics trajectory data, J. Chem. Theory Comput. 9 (7) (2013) 3084–3095.
[31] B.R. Miller, T.D. McGee Jr, J.M. Swails, MMPBSA. py: An efficient program for end-state free energy calculations, J. Chem. Theory Computat. 8 (9) (2012) 3314.